CHEMISTRY OF MATERIALS

pubs.acs.org/cm Article

Platinum ω-Alkenyl Compounds as Chemical Vapor Deposition Precursors: Synthesis and Characterization of $Pt[CH_2CMe_2CH_2CH{=}CH_2]_2$ and the Impact of Ligand Design on the Deposition Process

Sumeng Liu, Zhejun Zhang, Danielle Gray, Lingyang Zhu, John R. Abelson, and Gregory S. Girolami*

Cite This: *Chem. Mater.* 2020, 32, 9316–9334 Read Online

ACCESS | Metrics & More | Article Recommendations | Supporting Information

ABSTRACT: We describe the synthesis and characterization of three platinum(II) ω-alkenyl complexes of stoichiometry $Pt[CH_2CMe_2(CH_2)_xCH{=}CH_2]_2$ where *x* is 0, 1, or 2, as well as some related platinum(II) compounds formed as byproducts during their synthesis. The ω-alkenyl ligands in all three complexes, *cis*-bis(η^1,η^2-2,2-dimethylbut-3-en-1-yl)platinum (**2**), *cis*-bis(η^1,η^2-2,2-dimethylpent-4-en-1-yl)platinum (**3**), and *cis*-bis(η^1,η^2-2,2-dimethylhex-5-en-1-yl)platinum (**4**), bind to Pt by means of a Pt–alkyl sigma bond at one end of the ligand chain and a Pt–olefin pi interaction at the other; the olefins reversibly decomplex from the Pt centers in solution. The good volatility of **3** (10 mTorr at 20 °C), its ability to be stored for long periods without decomposition, and its stability toward air and moisture make it an attractive platinum chemical vapor deposition (CVD) precursor. CVD of thin films from **3** shows no nucleation delay on several different substrates (SiO_2/Si, Al_2O_3, and VN) and gives films that are unusually smooth. At 330 °C in the absence of a reactive gas, the precursor deposits platinum containing 50% carbon, but in the presence of a remote oxygen plasma, the amount of carbon is reduced to below the Rutherford backscattering spectroscopy (RBS) detection limit without affecting the film smoothness. Under hot wall CVD conditions at 250 °C in the absence of a co-reactant, 72% of the carbon atoms in **3** are released as hydrogenated products (largely 4,4-dimethylpentenes), 22% are released as dehydrogenated products (all of which are the result of skeletal rearrangements), and 6% remain in the film. Some conclusions about the CVD mechanism are drawn from this product distribution.

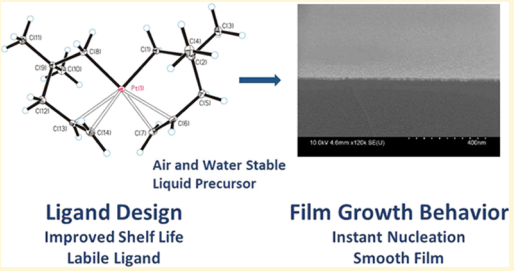

INTRODUCTION

Some 30 years ago, our research group was the first to show that the organoplatinum complex $(C_5H_5)PtMe_3$ was a useful precursor for the chemical vapor deposition (CVD) of platinum thin films.[1] Over the years, many other Pt CVD precursors have been described,[2−4] but a close variant of $(C_5H_5)PtMe_3$, the methylcyclopentadienyl complex $(C_5H_4Me)PtMe_3$, has become the most widely employed.[5] Like $(C_5H_5)PtMe_3$, it is stable toward air and moisture, it is thermally stable at room temperature, and its vapor pressure (53 mTorr at 23 °C) is relatively high.[6,7] Pure platinum films can be grown by CVD or atomic layer deposition (ALD) from $(C_5H_4Me)PtMe_3$ and several other precursors, provided that a reactive gas is present, such as hydrogen, oxygen, ozone, or an oxygen plasma;[6−11] these reactive gases assist in the removal of excess carbon from the films.

Today, the CVD[2−4,12,13] and atomic layer deposition (ALD)[14−17] of platinum thin films from organoplatinum precursors are of interest for a wide variety of applications, including the fabrication of gate electrodes[18] and other microelectronic structures,[8,19] as catalysts,[20−23] as a component of data storage media,[24] and as electrical contacts in medical devices.[25−27]

Though widely studied, one major drawback of $(C_5H_4Me)PtMe_3$ as a CVD precursor is that it suffers from long nucleation delays.[7,8,11,28,29] This problem can be traced to the high metal–ligand bond strengths and consequent high kinetic barriers associated with eliminating ligands from adsorbed $(C_5H_4Me)PtMe_3$ molecules.[29,30] Such elimination reactions typically occur more quickly on platinum surfaces than they do on the underlying substrate, owing to the highly catalytic nature of platinum.[5,8,31] As a result, deposition initiates to form islands on the surface, which subsequently grow rapidly. Similar island growth behavior has been observed for several other Pt CVD precursors.[10,32−36] Eventually, the islands coalesce, but the long nucleation delays, and resulting sparse

Received: August 6, 2020
Revised: October 2, 2020
Published: October 27, 2020

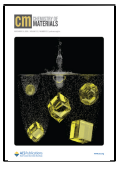

https://dx.doi.org/10.1021/acs.chemmater.0c03226
Chem. Mater. 2020, 32, 9316–9334

nucleation, mean that it is difficult to make continuous films that are also very thin; instead, at the point of full coalescence, the films are typically relatively thick and rough. Although the deposition of conformal Pt films has been achieved by means of an alternating ALD/oxygen plasma process from $(C_5H_4Me)PtMe_3$, nucleation delays of ~50 cycles are still observed.[31]

The nucleation delay problem can potentially be resolved by employing a precursor whose ligands can more easily eliminate than those in $(C_5H_4Me)PtMe_3$.[16] For example, the "open-Cp" precursor (2,4-dimethylpentadienyl)(ethylcyclopentadienyl)-ruthenium(II) shows enhanced nucleation compared to bis(ethylcyclopentadienyl)ruthenium(II),[37] and the amino-alkene precursor dimethyl(*N*,*N*-dimethyl-3-buten-1-amine) platinum shows enhanced nucleation compared to (C_5H_4Me)-$PtMe_3$.[38]

In this context, we have previously described the square-planar platinum(II) precursor in which two coordination sites are occupied by weakly coordinating olefin groups: Pt-$[(CH_2)_3CH{=}CH_2]_2$ or *cis*-bis(η^1,η^2-pent-4-en-1-yl)platinum (**1**).[35] Although this pentenyl compound is highly volatile and affords relatively clean platinum films,[35] it decomposes thermally within 2 weeks at room temperature[35,39] and thus is not ideal as a CVD precursor. The thermal sensitivity stems from the availability of a low-barrier mechanism to eliminate a ligand: β-hydrogen elimination initiated by decomplexation of the olefin groups:

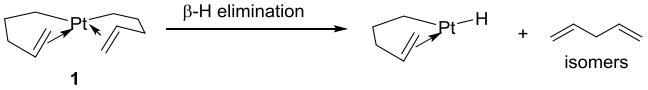

1

In the present study, we sought to prepare new platinum CVD precursors that are stable at room temperature but still retain the lability of the alkenyl ligands, with the idea that a low-barrier pathway for dissociation of a ligand would lead to fast nucleation.[40−42] Our strategy was to replace the β-hydrogen atoms in **1** with methyl groups: this "β-stabilization" strategy has long been employed to increase the thermal stability of organometallic complexes.[43−47]

We now report the synthesis and characterization of three new "β-stabilized" platinum complexes of stoichiometry $Pt[CH_2CMe_2(CH_2)_xCH{=}CH_2]_2$ where x is 0, 1, or 2: *cis*-bis(η^1,η^2-2,2-dimethylbut-3-en-1-yl)platinum (**2**), *cis*-bis(η^1,η^2-2,2-dimethylpent-4-en-1-yl)platinum (**3**), or *cis*-bis(η^1,η^2-2,2-dimethylhex-5-en-1-yl)platinum (**4**). We also describe the growth of the platinum films from **3**, which is a particularly interesting CVD precursor owing to its good volatility, its low melting point, its stability toward air and water, and its much longer shelf life compared to the "β-unstable" parent compound **1**. Notably, CVD of thin films from **3** shows no nucleation delay on several different substrates (SiO_2/Si, Al_2O_3, and VN) and gives films that are unusually smooth. In a separate paper, we will describe the mechanism by which **3** decomposes thermally in solution. Those results provide additional insights into the relationship between the structure of the precursor and the CVD growth kinetics and morphology of the resulting platinum thin films.

RESULTS AND DISCUSSION

Preparation of β-Stabilized Bis(ω-alkenyl)platinum(II) Complexes. In our earlier work, *cis*-bis(η^1,η^2-pent-4-en-1-yl) platinum (**1**) was generated by treatment of $(COD)PtCl_2$ (COD = 1.5-cyclooctadiene) with two equivalents of a Grignard reagent.[35] Similar reactions with the analogous β-stabilized Grignard reagents (or in one case with an alkyllithium) afford the corresponding compounds *cis*-bis-(η^1,η^2-2,2-dimethylbut-3-en-1-yl)platinum (**2**), *cis*-bis(η^1,η^2-2,2-dimethylpent-4-en-1-yl)platinum (**3**), and *cis*-bis(η^1,η^2-2,2-dimethylhex-5-en-1-yl)platinum (**4**). Compounds **2** and **3** are light yellow liquids, whereas **4** is a low-melting solid; all three compounds can be purified by column chromatography on silica gel with pentane as the eluent.

All three bis(ω-alkenyl)platinum compounds **2**, **3**, and **4** can be stored indefinitely under an argon atmosphere at −20 °C. Of the three, the dimethylbutenyl derivative **2** is the least stable: it reacts with air and water and decomposes within days at room temperature under Ar. Of intermediate stability is the dimethylhexenyl compound **4**, which is air and water stable but decomposes thermally in several days at room temperature. In contrast, the most stable is the dimethylpentenyl compound **3**, which can be stored at room temperature for 1 month in air with only slight darkening and with no observable changes in the NMR spectrum. Thus, **3** is far more thermally stable than its unmethylated analog **1**, which decomposes by β-hydrogen elimination over 2 weeks at room temperature.[39]

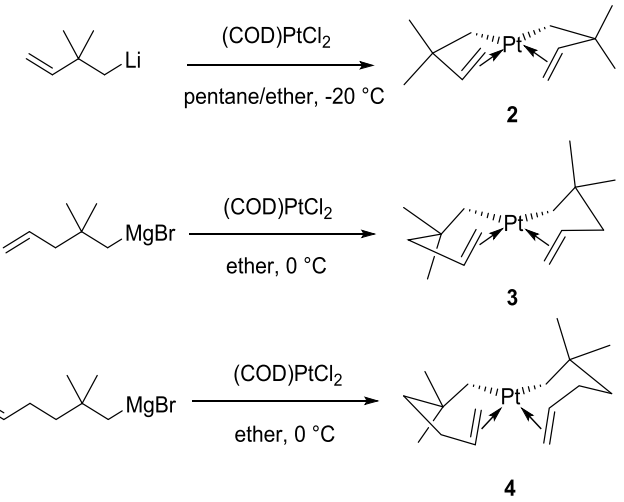

The melting points are ca. −15 °C for **2**, ca. 20 °C for **3**, and 46−47 °C for **4**; all three compounds **2**−**4** are volatile, with **2** having the highest volatility. Such low melting points are useful for CVD precursors because the delivery rate of liquid precursors can be easily controlled and reproduced.[3,7] The vapor pressure of **3**, which is 12 mTorr at 23 °C and 250 mTorr at 80 °C, follows the equation $\log p = 6.19 - 2400/T$ (pressure is in Torr and temperature is in K). The vapor pressure of **3** is only slightly lower than that of the commercial precursor $(C_5H_4Me)PtMe_3$, which has P_{vap} = 53 mTorr at 23 °C.[7] The enthalpy of evaporation of **3**, ΔH_{vap} = 11 ± 2 kcal mol^{-1} (see the Supporting Information, SI), is similar to the 10.5 ± 0.2 kcal mol^{-1} value reported for $(C_5H_4Me)PtMe_3$.[7]

Cyclooctadiene-Containing Byproducts. Treatment of $(COD)PtCl_2$ with the butenyl Grignard reagent, (2,2-dimethylbut-3-en-1-yl)magnesium bromide, gives poor yields of **2**; instead, the major product is the monoalkylated compound bromo(η^1-2,2-dimethylbut-3-en-1-yl)(1,5-cyclooctadiene)platinum (**5**). Good yields of **2** require the use of the corresponding alkyllithium reagent (see the Experimental Section).

https://dx.doi.org/10.1021/acs.chemmater.0c03226
Chem. Mater. 2020, 32, 9316−9334

Table 1. Crystallographic Data for the New Compounds

	2	3	4	5	6
formula	$C_{12}H_{22}Pt$	$C_{14}H_{26}Pt$	$C_{16}H_{30}Pt$	$C_{14}H_{23}BrPt$	$C_{20}H_{34}Pt$
FW (g mol^{-1})	361.38	389.44	417.49	466.32	469.56
λ (Å)	0.71073	0.71073	0.71073	0.71073	0.71073
T (K)	100	100	100	100	100
crystal system	monoclinic	monoclinic	monoclinic	monoclinic	monoclinic
space group	$P21/n$	$P21/c$	$C2/c$	$P2_1$	$C2/c$
a (Å)	6.2341(2)	5.8662(3)	6.0482(4)	9.7170(4)	18.3933(6)
b (Å)	10.3493(3)	21.591(1)	13.5208(8)	11.9545(5)	9.0744(3)
c (Å)	18.9360(6)	22.360(1)	19.287(1)	13.2835(6)	11.3108(4)
β (deg)	92.5422(8)	91.629(2)	95.364(2)	110.537(2)	104.951(1)
V (Å^3)	1220.52(7)	2830.9(2)	1570.3(2)	1445.0(1)	1823.9(1)
Z	4	8	4	4	4
ρ_{calcd} (g cm^{-3})	1.967	1.827	1.766	2.144	1.710
μ (mm^{-1})	11.455	9.884	8.916	12.450	7.687
R (int)	0.037	0.030	0.036	0.041	0.053
abs corr method	multi-scan	numerical	numerical	multi-scan	multi-scan
max/min transm factors	0.334/0.141	0.457/0.038	0.535/0.066	0.747/0.516	0.512/0.419
data/restraints/params	3042/0/140	7109/0/316	1952/0/90	11517/1/294	2274/0/101
GOF on F^2	1.231	1.170	1.210	1.070	1.125
R_1 [$I > 2\sigma(I)$][a]	0.0278	0.0142	0.0118	0.0189	0.0172
wR_2 (all data)[b]	0.0703	0.0293	0.0304	0.335	0.0374
max/min $\Delta\rho_{electron}$ (eÅ^{-3})	1.68/−2.27	0.62/−0.49	0.89/−0.78	0.93/−1.01	0.52/−1.13

[a] $R_1 = \sum ||F_o| - |F_c||/\sum|F_o|$. [b] $wR_2 = [\sum w(F_o^2 - F_c^2)^2/\sum(F_o^2)^2]^{1/2}$.

Table 2. Selected Bond Distances and Angles for the New Compounds[a]

	2	3	4	5	6
C═C/Å	1.370(8)	1.366(3)	1.373(3)	1.326(6)	1.324(4)
Pt−C_α/Å	2.068(5)	2.058(2)	2.077(2)	2.072(3)	2.083(2)
Pt−C_{olefin}[b]/Å	2.259(6)	2.301(2)	2.272(2)	N/A	N/A
Pt−C_{olefin}[c]/Å	2.296(6)	2.250(2)	2.257(2)	N/A	N/A
C_α−Pt−C_α'/deg	94.9(2)	88.81(8)	88.2(1)	89.8(2)[d]	88.6(1)
C_α−C_β−C_γ/deg	100.0(4)	106.6(2)	112.3(2)	110.7(3)	111.3(2)

[a] Some of the numbers given are averages over chemically equivalent bonds. [b] Methine carbon. [c] Methylene carbon. [d] C_α−Pt−Br angle.

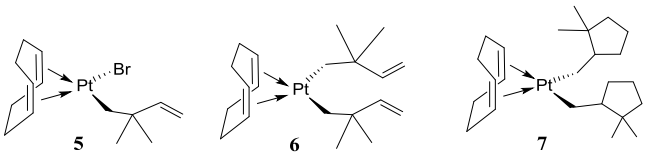

5 6 7

We also found that the adduct (1,5-cyclooctadiene)bis(η^1-2,2-dimethylbut-3-en-1-yl)platinum (**6**) is obtained when the butenyl compound **2** is sublimed at room temperature in the presence of ∼1 equiv of COD onto a cold (−80 °C) surface under vacuum. In both **5** and **6**, the olefin groups of the butenyl ligands are not coordinated to Pt. The COD adduct **6** is in equilibrium with **2** and free COD in solution: when pure **6** is dissolved at millimolar concentrations in toluene-d_8 at room temperature, it is almost completely dissociated to **2** and free COD (Figure S5.4). The temperature dependence of the equilibrium constant K_{eq} = [**6**]/([**2**][COD]) shows that ΔH = 5 ± 1 kcal mol^{-1} and ΔS = 29 ± 5 cal mol^{-1}·K^{-1} (Figure S5.6). The large entropy change is consistent with the dissociation of one particle to two:

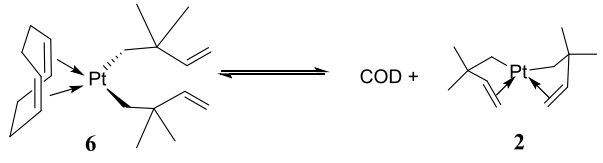

6 2

The reaction of (COD)$PtCl_2$ with the dimethylhexenyl Grignard reagent generates **4** in only 10% isolated yield because a second compound is also formed: (1,5-cyclooctadiene)bis[η^1-(2,2-dimethylcyclopentyl)methyl] platinum (**7**). This latter compound (which was isolated a mixture of three diastereomers) is the result of insertion of the olefin group into the Mg-C bond before alkylation of the Pt center. We show in the SI (Section 2) that **4** does not convert to **7** in benzene-d_6 in the presence of 1,5-cyclooctadiene, whereas the hexenyl Grignard reagent readily cyclizes (i.e., undergoes an 5-*exo-trig* insertion reaction).[48]

Solid-State Structures of the β-Stabilized Bis(ω-alkenyl)platinum(II) Complexes. Crystallographic data for compounds **2**−**6** are listed in Table 1, and selected bond distances and angles are given in Table 2. The structures of **2**−**4** (Figure 1) all contain two ω-alkenyl ligands in which the α-carbon atom is sigma-bound to platinum (η^1) and the C═C bond at the other end of the chain is pi-bound (η^2), as found previously for $Pt[(CH_2)_3CH{=}CH_2]_2$.[35]

Compounds **2**−**4** all adopt solid-state structures with (idealized) C_2 symmetries, in which the two α-carbon atoms are mutually *cis*. The C_α−Pt−C_α' angle of 94.9(2)° in the butenyl compound **2** is significantly larger than the ∼90° angles seen in the pentenyl and hexenyl compounds **3** and **4** (Table 2). This difference reflects the short chain length (and

https://dx.doi.org/10.1021/acs.chemmater.0c03226
Chem. Mater. 2020, 32, 9316−9334

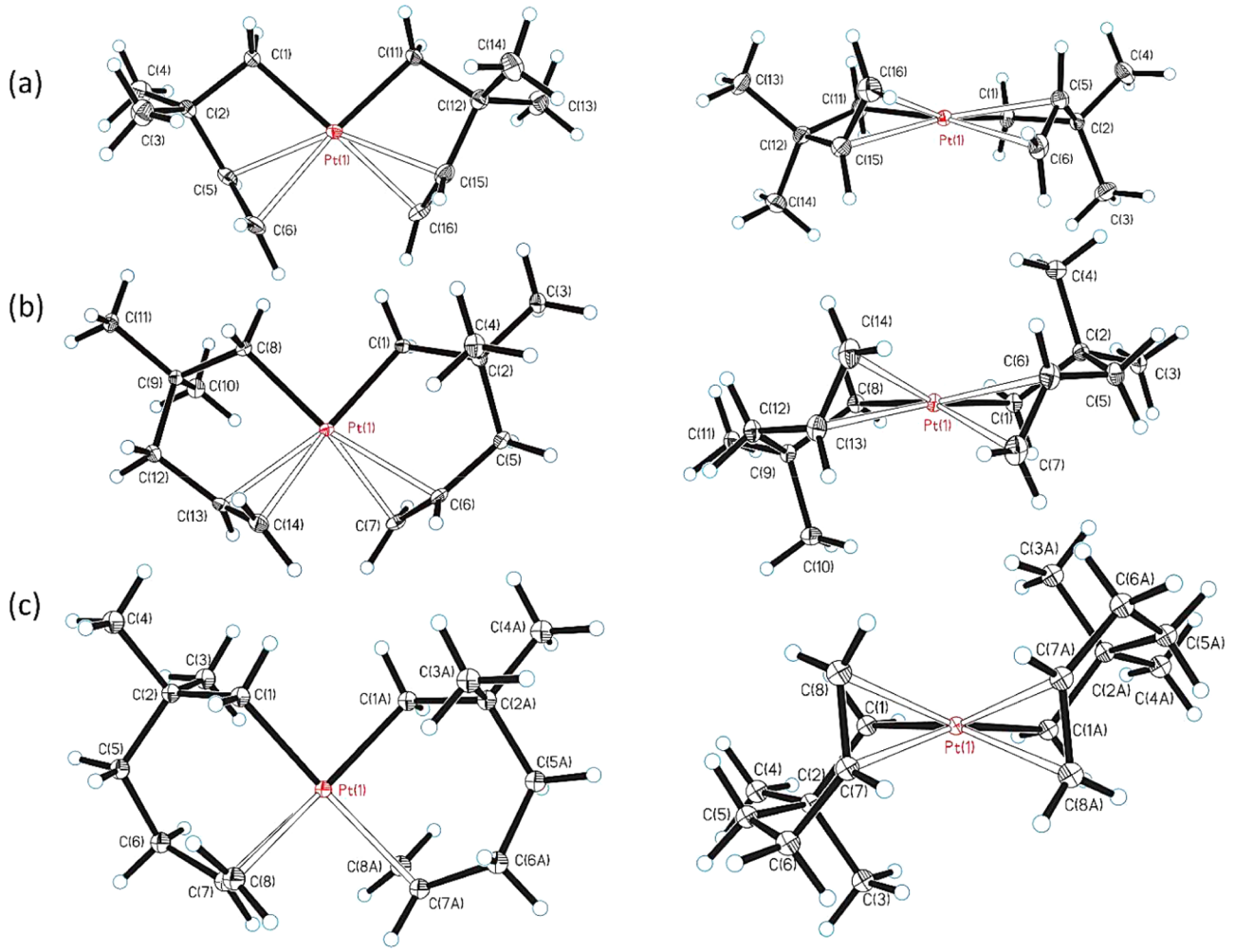

Figure 1. Left: Crystal structures of (a) *cis*-bis(η^1,η^2-2,2-dimethylbut-3-en-1-yl)platinum (**2**), (b) *cis*-bis(η^1,η^2-2,2-dimethylpent-4-en-1-yl)platinum (**3**), and (c) *cis*-bis(η^1,η^2-2,2-dimethylhex-5-en-1-yl)platinum (**4**). Right: Views showing different tilt angles of the C═C bond vectors with respect to the square plane in the butenyl compound **2**, the pentenyl compound **3**, and the hexenyl compound **4**. The ellipsoids are drawn at the 35% probability level, except the hydrogen atoms are depicted as arbitrarily sized spheres.

consequent small bite angle) of the chelating butenyl ligands in **2**.

The C_α–C_β–C_γ bond angles of 100.0(4) and 106.6(2)° in **2** and **3**, respectively, are compressed so as to enable the C═C bond to coordinate to platinum despite the short chain lengths. The C_α–C_β–C_γ bond angle of 112.3(2)° in **4** (for which the longer chain length reduces the ring strain) is similar to those in the COD adducts **5** and **6** (Figure 2), in which the ω-alkenyl ligands are unidentate and thus unaffected by ring strain.

The rings formed by the pentenyl groups in **3** adopt chair conformations. In contrast, twist-boat conformations are seen for most other complexes, including the unmethylated compound **1**, in which a bidentate ligand with a 5-atom backbone is bound to a metal by a sigma bond at one end of the chain and an η^2-C═C bond at the other.[49−59] We propose that the 2,2-dimethyl substituents in **3** cause the change in ring conformation, as has been seen in some related compounds.[60,61] Possibly for the same reason, the ω-alkenyl rings in the hexenyl compound **4** adopt boat-chair conformations, whereas in the butenyl compound **2**, they adopt idealized envelope conformations.

In four-coordinate platinum(II) olefin complexes, the C═C bond vector typically is normal to the square plane (we will call the angle between the C═C vector and the normal the tilt angle). For olefin complexes of d^8 square-planar metals, there is little electronic preference for any particular C═C orientation, but a tilt angle of 0° minimizes interligand steric repulsions.[62−65] In contrast, the C═C vectors in **2**–**4** are all tilted significantly away from this preferred orientation and instead form tilt angles of 52 and 35° (average = 44°) in the butenyl compound **2** (Figure 1), 29° in the pentenyl compound **3**, and 12° in the hexenyl compound **4**. For comparison, the tilt angles in the unmethylated pentenyl compound **1** were 34° and 23° (average = 29°).[35] The presence of two different tilt angles in **2** and also in **1** is undoubtedly a consequence of packing effects;[60] both compounds are completely symmetrical in solution (see below).

In the butenyl compound **2**, the short chain length clearly prevents the C═C bond vectors from being oriented in the normal direction. Similar conformational constraints are known to cause such tilting in other square-planar platinum(II) complexes, which in the extreme can cause coordinated C═C bonds to be oriented a full 90° away from the normal, i.e., the C═C bond lies in the square plane.[65,66] As the number of carbon atoms in the ligand backbone increases, there are more

https://dx.doi.org/10.1021/acs.chemmater.0c03226
Chem. Mater. 2020, 32, 9316−9334

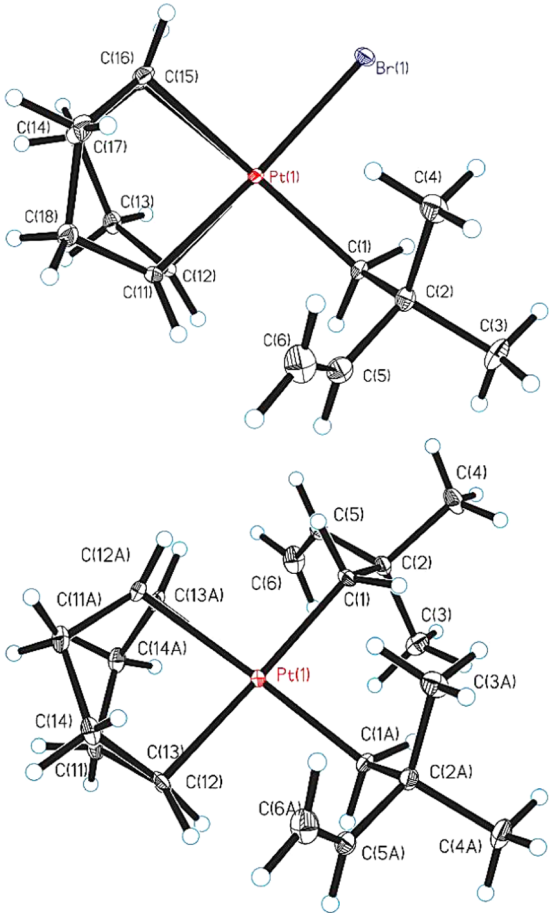

Figure 2. Top: Crystal structure of bromo(η^1-2,2-dimethylbut-3-en-1-yl)(1,5-cyclooctadiene)platinum (**5**). Bottom: Crystal structure of bis(η^1-2,2-dimethylbut-3-en-1-yl)(1,5-cyclooctadiene)platinum (**6**). The ellipsoids are drawn at the 35% probability level, except the hydrogen atoms are depicted as arbitrarily sized spheres.

conformational degrees of freedom and the C=C bond vectors form smaller tilt angles.

Unlike our pentenyl and hexenyl compounds **3** and **4**, however, many square-planar compounds are known in which an olefin at the end of a five- or six-atom chelating chain binds to a metal with a tilt angle of essentially zero.[49−59] We believe that this perpendicular structure is not adopted by the alkenyl ligands in **3** and **4** because it would lead to unfavorable inter- and intraligand repulsions involving the 2-methyl groups and the *cis*-double bonds.

The C=C bond lengths in compounds **2**−**4** of ∼1.37 Å (Table 2) are similar to the C=C bond lengths seen in other platinum(II) olefin complexes such as Zeise's salt.[67] The bonds are about ∼0.045 Å longer than the ∼1.325 Å C=C bond lengths seen for noncoordinated alkenes such as those in the COD adducts **5** and **6**. As expected, the C=C bond distances in **2**−**4** are similar to those in other platinum(II) η^1,η^2-pent-4-en-1-yl complexes in which the C=C bond is trans to non-π donors such as NHCs or phosphines,[52,60] but slightly shorter than those in which the C=C bond is trans to π donors such as chlorine or oxygen (∼1.40 Å).[49−51]

It is well known that coordination of olefins to metal centers causes the carbon atoms to rehybridize so that the four substituents are no longer co-planar with the C=C bond.[67] Interestingly, the olefinic methine group in the butenyl compound **2** remains planar despite having a Pt−C contact distance that is normal for Pt−olefin complexes. The planarity suggests that the Pt−C interaction with this carbon atom is largely nonbonding, a hypothesis that is consistent with the negligible Pt−C coupling constant to this carbon as seen in the solution NMR spectrum (see below).

The small elongation of the C=C bonds and the significant influence of steric and packing effects on the conformations of **2**, **3**, and **4** suggest that the olefin−Pt interactions are relatively weak in these complexes; we will return to this issue in a subsequent section.

Isomerism of the β-Stabilized Platinum(II) ω-Alkenyl Complexes in Solution. Interestingly, we find that the butenyl and hexenyl complexes **2** and **4** exist in solution as a mixture of two species,[68] even though only one species is observed in the solid state. For all three compounds **2**−**4**, three diastereomers are possible: two diastereomers of C_2 symmetry in which the two olefins present the same face to Pt (re−re or si−si; these two alternatives are enantiomers and thus give the same NMR spectrum) and one diastereomer of C_s symmetry in which the two olefins present different faces to Pt (si-e). For the rest of this discussion, we will refer to the re−re and si−si diastereomers as "the C_2 isomer" and the si−re diastereomer as "the C_s isomer."

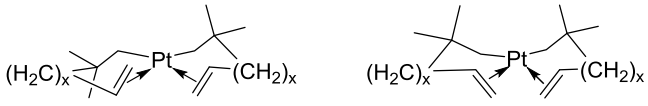

C_2 C_s

In the solid state, compounds **2**−**4** all adopt the C_2 structure. In solution, only a single isomer of the pentenyl compound **3** is evident from the NMR spectra, which certainly is also the C_2 structure (if the C_s isomer is present, its concentration is less than 1%). For solutions of the butenyl and hexenyl compounds **2** and **4**, however, significant amounts of both the C_2 and C_s isomers are present. Thus, in toluene-d_8 at room temperature, the ^{195}Pt NMR spectrum of **3** shows only one singlet at δ −3777, whereas the ^{195}Pt NMR spectrum of **2** shows two peaks at δ −4019 and δ −4110, in a ratio of approximately 2:1, and the ^{195}Pt NMR spectrum of **4** shows two peaks at δ −3778 and δ −3797, in a ratio of approximately 10:1 (Figure 3). For the rest of this discussion, we will assume that the predominant species in solution for **2** and **4** is the C_2 isomer seen in the

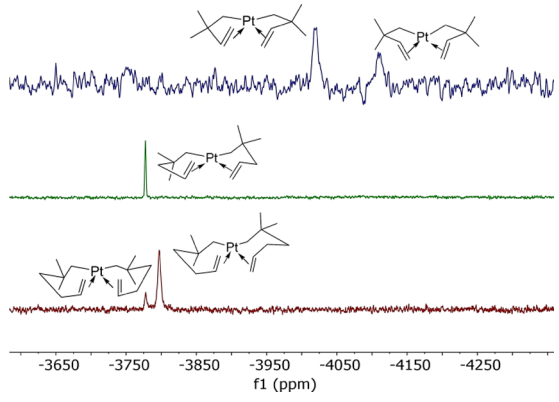

Figure 3. ^{195}Pt NMR spectra of the butenyl compound **2** (top), the pentenyl compound **3** (middle), and the hexenyl compound **4** (bottom) at 20 °C in toluene-d_8. Two isomers (C_2 and C_s) exist in solution for **2** and **4**, but not for the pentenyl compound **3**.

https://dx.doi.org/10.1021/acs.chemmater.0c03226
Chem. Mater. 2020, 32, 9316−9334

solid state; as we will see, this assumption can explain the relative amounts of the two isomers as a function of chain length, whereas the opposite assumption cannot.

The presence in solution of only the C_2 isomer for the pentenyl compound **3** but both the C_2 and C_s isomers for **2** and **4** is also evident in the ^{1}H and ^{13}C{^{1}H} NMR spectra. Thus, the ^{1}H NMR spectrum of the butenyl compound **2** at −60 °C in toluene-d_8 shows twice the number of expected peaks (discussed in detail below), which can be assigned to the presence of two isomers in a 2:1 concentration ratio (Figure 4). A variable temperature NMR study of **2** shows that the

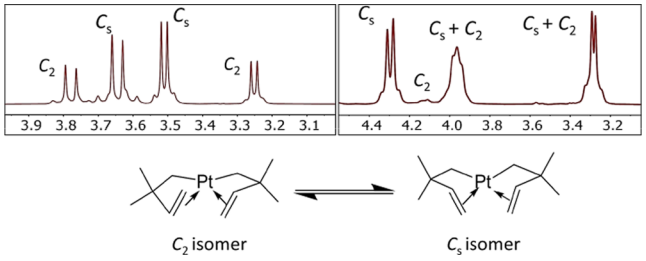

Figure 4. ^{1}H NMR spectra in the olefinic region of the butenyl compound **2** (top left) and the hexenyl compound **4** (top right) at −60 °C in toluene-d_8. The C_2/C_s isomer ratios for **2**, **3**, and **4** are 1.9:1, >100:1, and 11:1, respectively.

relative amount of the minor (C_s) isomer increases slightly with temperature. Fitting the temperature dependence of the equilibrium constant $K_{eq} = [C_2\text{-}\mathbf{2}]/[C_s\text{-}\mathbf{2}]$ to the van't Hoff equation gives the following parameters: $\Delta H = -0.3 \pm 0.5$ kcal mol^{-1}, $\Delta S = 0 \pm 2$ cal mol^{-1}·K^{-1} (Figure S6.2). The small values for the enthalpy and entropy changes show that the two isomers are rather similar thermodynamically. Likewise, two isomers are also seen in the low-temperature ^{1}H and ^{13}C{^{1}H} NMR spectra of the hexenyl compound **4**, in approximately a 10:1 ratio. Fitting the temperature dependence of the equilibrium constant $K_{eq} = [C_2\text{-}\mathbf{4}]/[C_s\text{-}\mathbf{4}]$ to the van't Hoff equation gives $\Delta H = -0.8 \pm 0.5$ kcal mol^{-1}, $\Delta S = 1 \pm 2$ cal mol^{-1}·K^{-1} (Figure S6.14). The C_2 isomer is favored over the C_s isomer at room temperature by a free-energy difference ΔG of 0.3 ± 0.8 kcal mol^{-1} for **2** and by 1.1 ± 0.8 kcal mol^{-1} for **4**.

The C_s isomer is not observed for the pentenyl compound **3**. We propose that, for all three compounds, the energy of the minor isomer is dictated by the energy penalty that arises from steric repulsions between the two olefin groups. The small bite angle of the butenyl ligand in **2** means that the two olefins are far from one another, so that the nonbonded repulsion between the two olefin groups in each of the isomers is small. The result is that both isomers have about the same energy. The longer chain length of the hexenyl ligand in **4** means that the olefinic C=C vectors in **4** are nearly perpendicular to the square plane of the Pt center; the nonbonded repulsions between the two olefin groups in the C_2 and C_s isomers are probably not small, but owing to the perpendicular orientation they are likely to be rather similar, so that again the two isomers have about the same energy.

For the pentenyl compound **3**, the bite angle is sufficiently large to place the olefins in close proximity in the C_s isomer, but the conformational constraints of the β-methyl groups and the five-carbon backbone make steric clashing of the olefin groups unavoidable, particularly for the C_s isomer of **3**. The energy of this isomer is therefore higher, which results in it being present in solution in amounts too small to detect by NMR spectroscopy. Nevertheless, as we will show below, this isomer must be present transiently in solution, as an intermediate in an intramolecular dynamic process.

Structure and Bonding of the β-Stabilized Platinum-(II) ω-Alkenyl Complexes in Solution. The ^{1}H and ^{13}C NMR resonances in **2**−**4** have been assigned based on the peak patterns, coupling constants, and one-dimensional (1D) nuclear Overhauser effect spectroscopy (NOESY) NMR spectra (see Figure 5). For all three compounds, the following

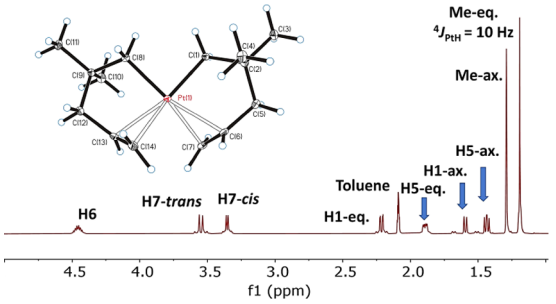

Figure 5. ^{1}H NMR spectrum of the pentenyl compound **3** in toluene-d_8 at −20 °C.

discussion will initially focus on the spectra of the C_2 isomer, which is the only isomer present for the pentenyl compound **3**, and is the major isomer for the butenyl and hexenyl compounds **2** and **4**. All of the NMR data (reported below for solutions in toluene-d_8) are consistent with structures in which the alkenyl ligands coordinate to Pt in an η^1,η^2 fashion. Thus, the ^{1}H NMR spectra of the C_2 isomers of **2**−**4** each display three signals between δ 3 and 5, which are assigned to the olefinic protons (Table 3). The shielded chemical shifts and the diminished $^3J_{HH}$ coupling constants (compared to those seen for free olefins) clearly show that the C=C bonds are coordinated to platinum in solution.[35,55−59,69,70] In the ^{13}C{^{1}H} NMR spectrum of the butenyl compound **2** at −60 °C, small Pt−C coupling constants are observed for the olefinic carbons: $^1J_{PtC}$ is 26 Hz for the terminal methylene

Table 3. Selected ^{1}H and ^{13}C NMR Data for the C_2 Isomers of the Butenyl Compound 2, the Pentenyl Compound 3, and the Hexenyl Compound 4 in Toluene-d_8 at 20 °C Unless Otherwise Specified

	2[a]	3	4
^{1}H δ (α-CH$_2$)	1.32, 0.91	2.25, 1.64	2.30, ~1.80[b]
^{1}H $^2J_{PtH}$ (α-CH$_2$)/Hz	86, 105	37, 103	62, 101
^{1}H δ (−CH=)	4.39	4.51	~4.14[b]
^{1}H δ (=CH$_2$)	3.65, 3.51	3.57, 3.40	4.28, 3.39
^{1}H $^3J_{HH}$ (olefinic)/Hz	15.2, 8.8	14.7, 8.0	15, 9.1
^{13}C δ (α-CH$_2$)	5.46	43.3	46.7
^{13}C $^1J_{PtC}$ (α-CH$_2$)/Hz	610	844	861
^{13}C δ (−CH=)	97.37	104.67	104.51
^{13}C δ (=CH$_2$)	74.76	88.76	82.86
^{13}C $^1J_{PtC}$ (−CH=)/Hz	0	16	20[c]
^{13}C $^1J_{PtC}$ (=CH$_2$)/Hz	26	29	28[c]

[a]At −60 °C. At room temperature, the two isomers are exchanging rapidly. [b]Overlapping with other resonances. [c]At −70 °C. The ^{195}Pt satellites for the olefinic carbons of **2** in the low-temperature ^{13}C{^{1}H} NMR spectrum are broad owing to chemical shift anisotropy,[73] so these Pt−C coupling constants are somewhat less precise.

https://dx.doi.org/10.1021/acs.chemmater.0c03226
Chem. Mater. 2020, 32, 9316−9334

carbon and 0 Hz (!) for the methine carbon. This zero coupling constant to the methine carbon is consistent with the observation in the solid state that this carbon atom is planar and apparently unhybridized. One possibility is that, owing to the constraints of the short chain length, the methine p-orbital is located close to the nodal surfaces of the linear combinations of the valence orbitals on Pt; as a result, the overlap of the methine carbon with Pt is relatively weak.[71,72]

Small $^1J_{PtC}$ coupling constants are also observed in the $^{13}C\{^1H\}$ NMR spectra of the pentenyl compound **3** (29.4 Hz for the methylene carbon and 17 Hz for the methine carbon at 20 °C) and the hexenyl compound **4** (20 Hz for the methylene carbon and 28 Hz for the methine carbon at −70 °C). The small Pt−C coupling constants in **2**−**4** show that the C═C bonds remain bound to platinum in solution, but suggest that the interactions are relatively weak.

We describe all of the $^1J_{PtC}$ coupling constants to the olefin groups in **2**−**4** as "small" because in other platinum(II) *cis*-dialkyl diolefin complexes they are usually much larger: 55 Hz in (COD)$PtMe_2$, 46 Hz in the norbornadiene compound (NBD)$PtMe_2$,[74] and 44.6 Hz in the neopentyl compound (COD)$Pt(CH_2CMe_3)_2$.[75] Interestingly, the $^1J_{PtC}$ coupling constants to the olefinic carbons in **3** are also smaller than those of 50 and 40 Hz in the unmethylated analog $Pt[(CH_2)_3CH{=}CH_2]_2$, **1**.[76] This latter comparison suggests that the 2,2-dimethyl substitution in complexes **2**−**4** weakens the Pt−olefin bonding, perhaps by a combination of electronic factors (the trans influence of the neo-alkyl groups is larger than that of *n*-alkyl groups)[77] and steric factors (the 2-methyl groups force the rings to adopt conformations that are less favorable for Pt−olefin overlap).

Long-range Pt−H couplings to ligand protons in platinum complexes are known to follow a Karplus-type dependence on the torsional angle between the Pt−C and C−H bonds,[78,79] and we can use this dependence to assign the ^1H NMR resonances in **2**−**4**. For example, in the ^1H NMR spectrum of the pentenyl compound **3** at −20 °C, one of the α-CH_2 protons, one of the β-methyl groups, and one of the γ-CH_2 protons, exhibits a large J_{Pt-H} coupling constant, whereas the partner group in each diastereotopic pair shows little or no observable J_{Pt-H} coupling (in fact, **3** shows a four-bond $^4J_{Pt-H}$ coupling of 10 Hz to the equatorial 2-Me group). If we assume that the pentenyl ligands adopt chair conformations as observed in the solid state (Figure 6), then the larger couplings can be assigned to the equatorial groups (which form torsion angles relative to the Pt−C bond that are close to 180°) and the smaller couplings to their axial counterparts (which describe torsion angles that are close to 90°). These assignments have been confirmed by a series of 1D NOE experiments (Figure S4.7).

The $^1J_{PtC}$ coupling constant to the α-CH_2 group of 610 Hz seen for the butenyl compound **2** is significantly smaller than those of 844 and 861 Hz observed for the pentenyl and butenyl compounds **3** and **4**, respectively. The latter are similar to the $^1J_{PtC}$ coupling constant of 844 Hz seen in the neopentyl complex (cod)$Pt(CH_2CMe_3)_2$.[75] The ^{13}C NMR chemical shift for the α-CH_2 group in **2** of δ 5.5 is also quite different from those of δ 43.3 and 46.7 seen for **3** and **4**. We attribute these differences to the short chain length of the butenyl ligand in **2**: the greatly perturbed interligand angles evidently affect the Pt−C σ interactions, as well as the values of the chemical shift tensor.[80]

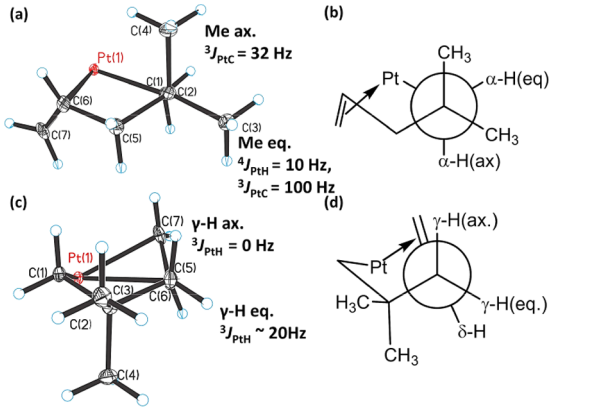

Figure 6. (a) View of the pentenyl compound **3** along the C_β−C_α bond, (b) Newman projection of **3** along the C_β−C_α bond, (c) view of **3** along the C_γ−C_δ bond, and (d) Newman projection of **3** along the C_γ−C_δ bond. In (a) and (c), the platinum atoms are in red and the carbon atoms are in black. Hydrogen atoms are depicted as arbitrarily sized spheres.

Coordination Dynamics of the Pt−Olefin Bond. In compounds **2**−**4**, the binding of the platinum atom to one face of the olefin makes the two hydrogen atoms of each -CH_2- unit in the alkenyl ring (and the two methyl groups of the CMe_2 unit) diastereotopic. At low temperatures, the ^1H NMR spectra show that these pairs of H atoms (or pairs of Me groups) are indeed chemically inequivalent, as mentioned above. For all three compounds, however, an exchange process occurs that causes the ^1H NMR peaks arising from these groups initially to broaden and then to coalesce as the temperature is raised. Because the terminal vinyl protons of **3** show no broadening, the only mechanism that can explain these exchange processes is decomplexation of the olefin from the Pt center and recoordination through the other face of the olefin;[81,82] such exchange processes have been called "alkene flipping".[83] This same exchange process also results in the exchange of the C_2 and C_s isomers of **2** and **4** and requires that the C_s isomer of **3** also be formed transiently in solution, although in amounts too small to detect. We note that similar exchange processes have been seen in other η^1,η^2-ω-olefin complexes of platinum.[84]

For the pentenyl compound **3**, which exists in solution exclusively as the C_2 isomer, the ^1H NMR line shapes of the diastereotopic methyl groups (Figure 7) were simulated in terms of a two-site exchange process to determine the olefin face exchange rate as a function of temperature.[85] A fit of 24 rates between 11 and 69 °C to the Eyring equation gives activation parameters of $\Delta H^{\ddagger}$ = 19 ± 1 kcal mol^{-1} and $\Delta S^{\ddagger}$ = 9 ± 3 cal mol^{-1}·K^{-1} for the exchange process between the methyl groups in **3** (Figure S6.11 and S6.12). Because the rate of exchange is half of the rate of olefin decomplexation (see the Experimental Section), the activation parameters for olefin decomplexation are $\Delta H^{\ddagger}$ = 19 ± 1 kcal mol^{-1} and $\Delta S^{\ddagger}$ = 10 ± 3 cal mol^{-1}·K^{-1}.

Similarly small but positive activation entropies of 12−14 cal mol^{-1}·K^{-1} seen for olefin face exchange processes in some 4-pentenyl zirconocene compounds[86,87] were proposed to indicate a mechanism in which the metal−olefin bond is broken without the concomitant association of solvent molecules (solvent-assisted mechanisms should have negative activation entropies). We propose, therefore, that olefin face exchange in **3** also occurs by breaking the platinum−olefin bond[41,88] without the involvement of solvent. The resulting

https://dx.doi.org/10.1021/acs.chemmater.0c03226
Chem. Mater. 2020, 32, 9316−9334

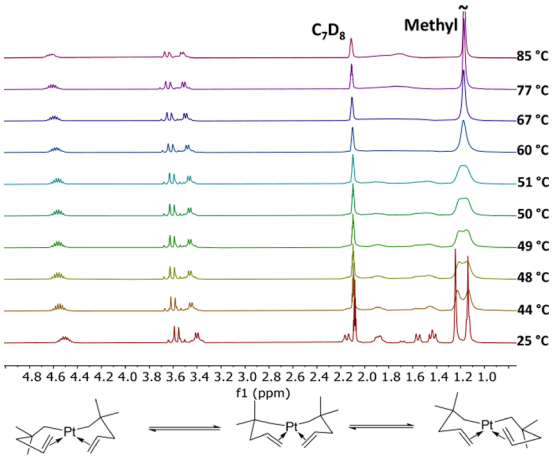

Figure 7. Variable-temperature (VT)-^{1}H NMR spectrum of the pentenyl compound **3** in toluene-d_8.

intermediate is either a 3-coordinate species with an empty site (if the olefin simply dissociates)[89−91] or a 4-coordinate C−H σ complex (if the metal−olefin bond is broken but is replaced with an agostic interaction).[83,92,93] In fact, C−H σ complexes have been proposed as intermediates in olefin face exchange processes in certain d^6 rhenium[93] and d^0 zirconium[83,92,94] complexes. Compared to the ground-state η^2-olefin complex, the transition state that leads to the C−H σ-complex intermediate should have increased degrees of freedom due to the expansion of the ring size, so that a small and positive entropy of activation is expected.

For the butenyl and hexenyl compounds **2** and **4**, analysis of the ^{1}H NMR line shapes is more complicated because of the effects of coupling to platinum and also because these compounds exist in solution as a mixture of the C_2 and C_s isomers (in ratios of ∼2:1 and ∼10:1, respectively) some of whose ^{1}H NMR resonances overlap. For both compounds, we found that the rate is best determined by fitting the line shapes of selected ^{13}C{^{1}H} NMR resonances. For **2**, fitting of the olefin face exchange rate at 11 different temperatures between −46.4 and 22.2 °C to the Eyring equation gives $\Delta H^{\ddagger}$ = 13.8 ± 0.6 kcal mol^{-1} and $\Delta S^{\ddagger}$ = 4 ± 2 cal mol^{-1}·K^{-1} for the C_2 isomer and $\Delta H^{\ddagger}$ = 13.5 ± 0.6 kcal mol^{-1} and $\Delta S^{\ddagger}$ = 4 ± 2 cal mol^{-1}·K^{-1} for the C_s isomer (Figures S6.5−S6.9). For **4**, fitting of the olefin face exchange rate at 8 different temperatures between −2.8 and 33.6 °C to the Eyring equation gives $\Delta H^{\ddagger}$ = 17 ± 1 kcal mol^{-1}, $\Delta S^{\ddagger}$ = 5 ± 4 cal mol^{-1}·K^{-1} for the C_2 isomer and $\Delta H^{\ddagger}$ = 16 ± 1 kcal mol^{-1}, $\Delta S^{\ddagger}$ = 6 ± 4 cal mol^{-1}·K^{-1} for the C_s isomer (Figures S6.16−S6.18).

The solvent is unlikely to participate in these exchange processes: activation entropies for olefin face exchange in metal complexes of the 2-methylhex-5-en-2-olate ligand (which is structurally analogous to the 2,2-dimethylhex-5-en-1-yl ligand in **4** in terms of having the same chain length and similar conformational flexibilities) are ∼3−8 cal mol^{-1} K^{-1} when the exchange process is purely intramolecular, but are 8−12 eu more negative if solvent plays a role.[81,82]

The 4 to 10 cal mol^{-1}·K^{-1} entropies of activation for **2**, **3**, and **4** (Table 4) indicate that olefin face exchange in all three ω-alkenyl compounds takes place by a mechanism involving a transition state in which the metal−olefin bond is broken but (most likely) replaced with an agostic interaction between Pt and one of the ω-hydrogen atoms.[81,83,93,95−98] At 20 °C, the rate of the olefin decomplexation increases in the following order: 6 s^{-1} for the pentenyl compound **3**, ∼40 s^{-1} for the hexenyl compound **4**, and ∼3000 s^{-1} for the butenyl compound **2**. Notably, the rate of thermal decomposition of the platinum η^1,η^2-2,2-dimethyl-ω-alkenyl complexes at room temperature increases in the same order (i.e., **3** < **4** < **2**). This correlation suggests that the intermediate formed during the olefin face exchange is also an intermediate in the thermolysis pathway.

Owing to its higher thermal stability compared to the other new alkenyl compounds, the pentenyl compound **3** shows the best potential as a CVD precursor, a topic to which we now turn.

Cold Wall Chemical Vapor Deposition of Thin Films from 3. Cold wall CVD experiments were performed in a high-vacuum chamber described elsewhere,[99,100] and the onset of nucleation and film growth were monitored by real-time spectroscopic ellipsometry (SE).[101] Film thicknesses were measured by scanning electron microscopy (SEM), and growth rates (in atoms per area) were measured by Rutherford backscattering spectroscopy (RBS). The films were grown from the pentenyl compound **3**, which was kept in a reservoir maintained at 75 °C and transported to the growth chamber with an argon carrier gas.

We find that, at substrate temperatures between 275 and 350 °C, smooth and reflective films can be grown from **3** on various substrates (SiO_2/Si, Al_2O_3, and VN). For example, on a SiO_2/Si substrate at 330 °C, a 17 nm film with a rms roughness of 1.7 nm was deposited in less than 10 min (Figure 8). Interestingly, unlike growth from $(C_5H_4Me)PtMe_3$, which shows significant nucleation delays,[7,8,11,28,29] growth from **3** occurs without delay on all substrates tested (Figure 8).

While maintaining the same substrate reservoir temperature and carrier gas flow rate, the rate of deposition (Å/min) increases exponentially with an increasing temperature between 275 and 330 °C (Figure S8.2); this result shows that growth under these conditions is in the reaction-limited regime. The deduced activation energy of 18 kcal/mol (0.78 eV) is considerably smaller than the >1.5 eV activation energy seen for growth from $(C_5H_4Me)PtMe_3$.[8] In addition, the onset temperature for CVD growth from **3** is ∼25 °C lower than that of ∼300 °C for $(C_5H_4Me)PtMe_3$.[5] All of these observations are consistent with the conclusion that **3** is a more reactive molecule under CVD conditions than the cyclopentadienyl

Table 4. Activation Parameters for C═C Bond Decomplexation in Toluene-d_8, and Correlation With Thermal Stability, for the Butenyl Compound 2, the Pentenyl Compound 3, and the Hexenyl Compound 4

	2	3	4
$\Delta H^{\ddagger}$, kcal mol^{-1}	13.8(6), C_2 13.5(6), C_s	19(1)	17(1), C_2 16(1), C_s
$\Delta S^{\ddagger}$, cal mol^{-1}·K^{-1}	4(2), C_2 4(2), C_s	10(3)	5(4), C_2 6(4), C_s
$\Delta G^{\ddagger}$, kcal mol^{-1} at 20 °C	12.6(8), C_2 12.3(8), C_s	16(1)	16(2), C_2 14(2), C_s
thermal stability at 20 °C	unstable	stable for weeks	unstable

https://dx.doi.org/10.1021/acs.chemmater.0c03226
Chem. Mater. 2020, 32, 9316−9334

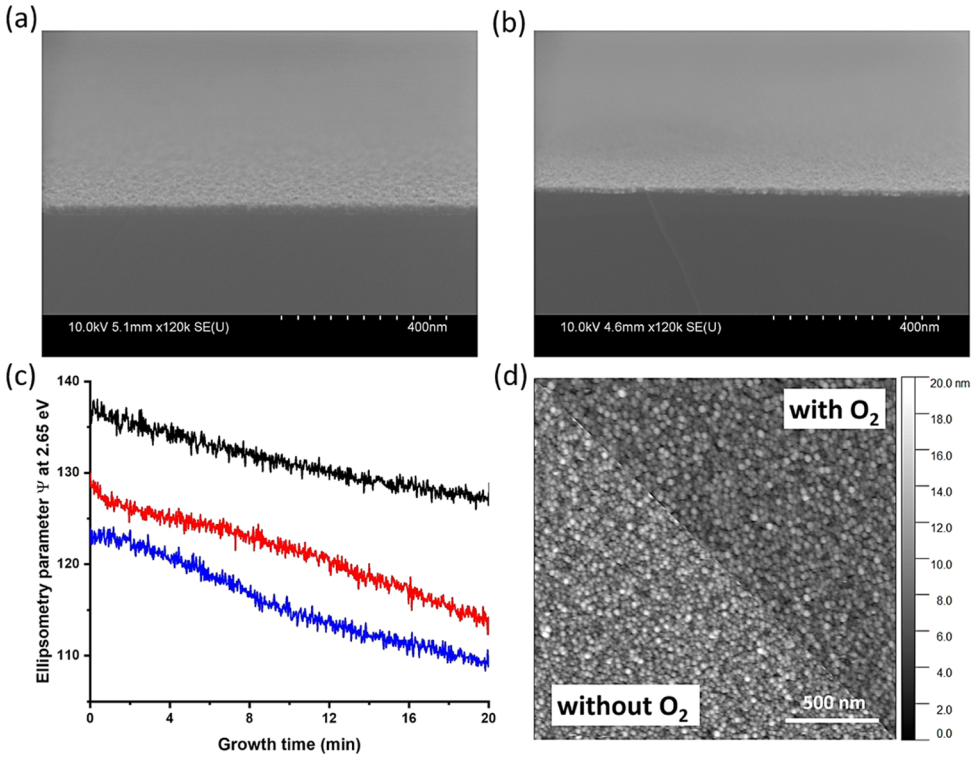

Figure 8. (a) SEM image of a Pt film grown from the pentenyl compound **3** on silicon at 330 °C (thickness: 19 nm); (b) SEM image of a Pt film grown from the pentenyl compound **3** on silicon at 330 °C in the presence of an oxygen plasma (thickness: 11 nm); (c) real-time ellipsometry curve (at 2.65 eV) of Pt growth at 330 °C on SiO_2/Si, VN, and Al_2O_3. The platinum precursor is introduced at the time of 0. The ellipsometry signal responds immediately to the introduction of the precursor, which suggests that there is no nucleation delay on these three substrates; (d) atomic force microscopy (AFM) image of a Pt film grown without and with oxygen plasma from the pentenyl compound **3** at 330 °C on an Al_2O_3 substrate.

compound, as expected owing to the presence of the labile ω-alkenyl groups.

As is typically seen for organoplatinum CVD precursors, the films obtained from **3** contain both platinum and carbon when the depositions are conducted in the absence of oxidative or reductive co-reactants. RBS analysis shows that the films grown under such conditions consist of ∼50 atom % platinum with the balance being carbon. Because of the presence of the latter,[102−105] a 12 nm film deposited at 330 °C on Al_2O_3 has a relatively high resistivity of 830 $\mu\Omega$·cm vs the 10.6 $\mu\Omega$·cm value seen for bulk platinum.[10]

Remote Oxygen Plasma-Assisted Chemical Vapor Deposition of 3. The quality of films grown by CVD from organoplatinum precursors is usually improved, and the deposition rate is often increased, by addition of oxidants or reductants such as O_2 or H_2 to the gas stream, which react with excess carbon to remove it as CO_x.[3,8,106] or C_xH_y.[7,10] We find, however, that addition of reactant gases such as O_2 or H_2 to a flux of **3** has almost no effect on the deposition rate. This finding suggests that the Pt surface generated from **3** is poisoned in such a way that it is unable to activate these molecules. We therefore investigated lowering the carbon content of the films by employing a reactant that does not rely on the catalytic ability of the platinum surface: atomic oxygen generated by a low-power remote plasma.[9] Using the same cold wall equipment, we found that deposition from **3** at 330 °C in the presence of a remote oxygen plasma (see the experimental section) also occurs with no nucleation delay, and that the rate of deposition is increased to ∼220% of its value in the absence of the plasma.

The purity, crystallinity, and resistivity of the film grown in the presence of the oxygen plasma also show significant improvements (Figure S8.3 and S8.4): the oxygen and carbon contents are below the RBS detection limit (variously estimated to be between 5[9] and 30%) vs the ∼50% carbon content seen for the films grown from **3** in the absence of a plasma. The films grown in the presence of the remote oxygen plasma contain nanocrystalline platinum with crystalline domains of ∼7 nm in size (Figure S8.4) and are reasonably smooth: the rms roughness of 2.2 nm is comparable with the 1.7 nm value seen in the absence of the plasma (Figure 8). The use of the oxygen plasma also lowers the resistivity from 830 to 450 $\mu\Omega$·cm for a 12 nm film deposited on Al_2O_3. It may prove possible to obtain films with even faster growth rates, lower carbon contents, and lower resistivities by employing a stronger plasma source or a different oxidant such as ozone.

Hot Wall Chemical Vapor Deposition of Thin Films from 3. To obtain information about the chemistry that occurs during the CVD growth from **3**, CVD experiments were performed in a static vacuum (∼10 mTorr) vertical hot wall deposition system equipped with a liquid nitrogen-cooled NMR tube[107] to trap the organic byproducts.[108] The precursor reservoir was kept at 75−80 °C to achieve reasonable growth rates, and the hot zone was heated either to 250 ± 10 or to 300 ± 10 °C. At both temperatures, smooth and reflective films can be grown on several different substrates (including silicon, gold, and glass).

The morphology and composition of the films grown in the static hot wall CVD apparatus are analogous to those obtained in the cold wall experiments in the absence of an oxygen

https://dx.doi.org/10.1021/acs.chemmater.0c03226
Chem. Mater. 2020, 32, 9316−9334

plasma (Figure S9.1−S9.6). Glancing angle XRD analysis shows that the ∼300 nm thick films grown at 250 °C contain nanocrystalline platinum, with crystalline domains ∼3.5 nm in size. The X-ray photoelectron spectra (XPS) show that the films grown on glass consist of 47% Pt, 40% C, and 13% O and the films grown on gold consist of 56% Pt, 38% C, and 5% O (the oxygen probably coming from postgrowth air exposure). In addition, for a film grown at 250 °C on glass, the electrical resistivity was 950 $\mu\Omega$-cm, which is similar to the conductivity of the films grown at 330 °C in the cold wall apparatus.

Quantitative ^{1}H NMR spectroscopy shows that the principal organic products generated at 250 °C under hot wall CVD conditions are 4,4-dimethyl-1-pentene (0.40 equiv per mole of **3** consumed), 4,4-dimethyl-2-pentene (0.80 equiv), and 2,2-dimethylpentane (0.24 equiv) (Figure S10.1−S10.7). Together, these three products account for 72% of the carbon atoms in **3**. All of these products are generated by adding hydrogen atoms to the 2,2-dimethylpentenyl ligands in **3**. When this CVD experiment is repeated in an apparatus whose surfaces have been deuterated (by treatment first with 2 M NaOD in D_2O and then with 2 M DCl in D_2O), the organic byproducts contain no deuterium above natural abundance levels, as judged by ^{2}H NMR spectroscopy. This experiment shows that the hydrogen that appears in the hydrogenated ligands does not come from adventitious sources such as the walls of the CVD chamber and must instead come from the precursor. Together, these experiments show that, when **3** is thermolyzed at 250 °C under CVD conditions, 72% of the pentenyl ligands are converted to C_7 products (4,4-dimethylpentene isomers and 2,2-dimethylpentane) by acquiring hydrogen atoms from the remaining 28% of the pentenyl ligands. In other words, some of the pentenyl ligands must be dehydrogenated by C−H bond activation, a process that readily occurs on Pt surfaces at these temperatures.[5,109−115]

Most of the pentenyl ligands that are dehydrogenated under CVD conditions at 250 °C are also released as volatile organic products. Among these dehydrogenated byproducts are the C_7 hydrocarbons 1,1-dimethyl-3-methylenecyclobutane (0.04 equiv per mole of **3** consumed), 1,3,3-trimethylcyclo-1-butene (0.06 equiv), 2,4-dimethyl-1,3-pentadiene (0.08 equiv), 1,1-dimethyl-2-methylenecyclobutane (0.06 equiv), and toluene (0.02 equiv) (See Supporting Information, Section S10). For all of these compounds, the dehydrogenation is accompanied by a rearrangement of the pentenyl skeleton by means of breaking and/or making C−C bonds. These dehydrogenated C_7 products, together with the small amount of isobutylene and higher-molecular-weight (most likely C_{14}) products formed, account for 22% of the carbon atoms in **3**. Combined with the 72% of the carbon atoms in **3** that are released as hydrogenated hydrocarbons, we find that 94% of the carbon atoms are released during CVD as volatile byproducts; the remaining 6% of the carbon atoms, or about one carbon atom per Pt, remain in the Pt film. The finding that just under one carbon atom per platinum is retained in the film is consistent with the XPS results.

In summary, the NMR and XPS data enable us to determine what happens to essentially all of the atoms in the precursor under CVD conditions; the stoichiometry of the reaction is shown in Scheme 1.

This product distribution is consistent with a mechanism in which about a quarter of the dimethylpentenyl ligands dehydrogenate on the surface.[5,109−114] The liberated hydrogen atoms combine on the surface with the other (nondehydrogenated) dimethylpentenyl ligands to produce 4,4-dimethylpentenes and 2,2-dimethylpentane, which dissociate from the surface and are carried away.

Scheme 1. Fate of the Carbon and Hydrogen Atoms during the CVD of the Films from the Pentenyl Precursor 3[a]

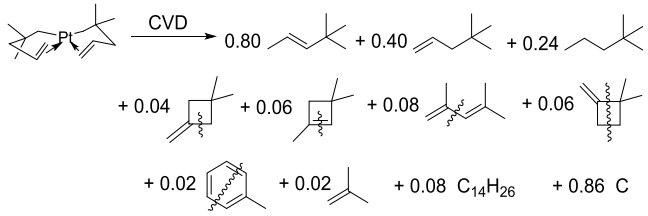

[a]The products that are the result of skeletal rearrangements are indicated with the wavy lines.

In contrast, the dehydrogenated ligands have no easy pathway to desorb from the surface because the 2,2-dimethyl substituents block low-energy pathways such as β-hydrogen elimination and formation of conjugated dienes. Other possible dehydrogenation products, such as acetylenes or allenes, are either not formed or are too strongly bound to the surface to desorb. Instead, the only way in which the dehydrogenated ligands from **2** can desorb from the surface is by undergoing processes that involve making or breaking C−C bonds, reactions that are known to occur on Pt surfaces.[113,116] In the present case, these skeletal rearrangements lead to the desorption of methylenecyclobutanes, cyclobutenes, pentadienes, and toluene, as well as isobutylene.

We conclude this section with a comparison of the CVD behavior of the unmethylated compound **1** and its β-stabilized analog **3**. In contrast to the byproduct distribution seen for **3** (which consists mostly of hydrogenated ligands), for the unmethylated analog **1**, both hydrogenated ligands (pentene isomers) and dehydrogenated ligands (pentadiene isomers) are generated in roughly equal amounts.[35] A key attribute is that both types of products (hydrogenated ligands and dehydrogenated ligands) have low-energy pathways to form volatile desorbates. The ease of removing both hydrogenated and dehydrogenated ligands from the surface is consistent with the relatively low carbon content (Pt/C ratio of ∼4.6:1) in the films grown from **1** in the absence of co-reactants. Compared to the CVD of **3**, the rapid desorption of most of the ligands during the CVD of **1** should generate a more active Pt surface, which will catalyze additional deposition from **1**. Such autocatalytic behavior should lead to the formation of rough films because growth is faster than nucleation. In fact, rough films indicative of autocatalytic CVD are exactly what we see for **1**.[35]

Comparison of CVD Behavior of 3 and $(C_5H_4Me)PtMe_3$. There are three important differences in the CVD of Pt from **3** and from $(C_5H_4Me)PtMe_3$: (1) CVD from **3** initiates very rapidly, whereas growth from $(C_5H_4Me)PtMe_3$ suffers from lengthy nucleation delays, (2) co-flow of O_2 or H_2 has almost no effect on the rate of the film deposition from **3**, but greatly increases the rate of deposition from $(C_5H_4Me)PtMe_3$,[8] and (3) films obtained from **3** are very smooth, but those obtained from $(C_5H_4Me)PtMe_3$ are quite rough.

We attribute the difference in nucleation delay to the lability of the alkenyl ligands in **3**: specifically, we propose that decomplexation of the olefin groups from Pt, which we know has a low barrier, forms highly reactive Pt species[90] that serve as nucleation initiators. In contrast, $(C_5H_4Me)PtMe_3$ is

https://dx.doi.org/10.1021/acs.chemmater.0c03226
Chem. Mater. 2020, 32, 9316−9334

kinetically very inert and has no low-energy pathways to break a Pt−C bond; the result is a long nucleation delay in ALD and a higher activation energy for growth in CVD.[8]

To explain the other two differences, we note that CVD from organoplatinum precursors inevitably leads to the formation of carbonaceous adsorbates, and such species in turn are known to influence the reactivity of the surface.[116,117] In this context, we know that **3** and $(C_5H_4Me)PtMe_3$ leave a similarly large amount of carbon impurities in the film when used as single-source precursors.[10,118] Thus, the difference between these two precursors must not lie in the amount of carbon generated, but instead must reflect a difference in its chemical nature.

It is known that step sites on Pt surfaces are able to break H−H and C−H bonds[116,119] and promote the activation of O_2,[120] and that kink sites are able to break C−C as well as H−H and C−H bonds.[116] We propose that the inability of the Pt films grown from **3** to activate O_2 and H_2 arises because the step and kink sites become poisoned by the dehydrogenated pentenyl ligands, which cannot desorb unless they undergo a skeletal rearrangement. Although the kink sites can promote C−C bond activation and can be reactivated when the rearranged ligand desorbs, this reactivation is slow because the skeletal rearrangement has a high barrier. When the reactivated kink sites bind to another dehydrogenated ligand, they become temporarily deactivated again. The net effect is that both the step and kink sites are poisoned, so that the surface is largely unable to chemisorb O_2 or H_2.

The poisoning can also explain why the films obtained from this precursor are so smooth: the poisoning inhibits autocatalytic deposition of **3**, which is known to occur with most Pt precursors. The resulting slower deposition rate, combined with the fast nucleation rate, creates circumstances in which growth occurs by constant renucleation, a mechanism that is known to lead to enhanced film smoothness.[121]

Concluding Remarks. We have made three new platinum(II) compounds containing chelating ω-alkenyl ligands *cis*-bis(η^1,η^2-2,2-dimethylbut-3-en-1-yl)platinum (**2**), *cis*-bis(η^1,η^2-2,2-dimethylpent-4-en-1-yl)platinum (**3**), and *cis*-bis(η^1,η^2-2,2-dimethylhex-5-en-1-yl)platinum (**4**). All three compounds are dynamic in solution: the C═C bonds reversibly decomplex at rates that are fast on the NMR time scale, with the pentenyl compound **3** showing the slowest decomplexation rates and the greatest thermal stability.

In addition to being thermally stable under ambient conditions, compound **3** is volatile and stable toward air and water and as such is a potentially useful new CVD precursor for platinum. At temperatures of 275−350 °C in vacuum, it nucleates very well on SiO_2/Si, Al_2O_3, and VN to deposit highly smooth thin films; this behavior is unlike most other platinum CVD precursors, which generally form large particles due to nucleation delays and autocatalytic growth kinetics. Compared to $(C_5H_4Me)PtMe_3$, which exhibits long nucleation delays in both CVD[7] and ALD,[28] deposition from **3** is characterized by a much shorter nucleation delay. This effect is probably a consequence of the availability of a low-barrier process in **3** (initiated by olefin decomplexation) to initiate the CVD mechanism; no such low-barrier process is available for the $(C_5H_4Me)PtMe_3$ precursor. The fast rate of nucleation for **3** also makes it a promising CVD precursor to deposit Pt nucleation layers.

As is common for all organoplatinum CVD precursors, the films obtained from **3** contain both platinum and some carbon when the depositions are conducted in the absence of a co-reactant. Interestingly, by employing a remote oxygen plasma, the amount of carbon impurities is significantly reduced and the resistivity of the films is lowered, without significantly degrading the smooth film morphology. The formation of carbon impurities is related to the reactions that **3** undergoes under CVD conditions: activation of the C−H bonds of some of the pentenyl ligands leads to the formation of surface hydrogen atoms, which react with other ligands to generate 2,2-dimethylpentenes and 4,4-dimethylpentane. These hydrogenated species desorb from the surface, but the dehydrogenated 2,2-dimethylpent-4-en-1-yl ligands can desorb only by undergoing higher-energy skeletal rearrangements and, as a result, they deactivate surface sites that normally react with H_2 or O_2 and catalyze further deposition from **3**. This behavior is unlike that seen for other organoplatinum precursors, which show no such poisoning effect. Further evidence in support of a poisoning effect is that removal of the carbonaceous species through the use of an oxygen plasma leads to faster growth rates. The combination of fast nucleation and slow (i.e., non-autocatalytic) growth is what is responsible for the highly smooth films that are deposited from **3**.[122]

All in all, the results provide an interesting example of how ligand engineering can be used to develop CVD precursors that afford films with desired properties. In addition to tuning the reactivity of the precursor molecule itself, the design can also dictate what organic groups are delivered onto the surface and those groups can affect the film morphology by changing the reactivity of the surface.

EXPERIMENTAL SECTION

All experiments were carried out in a vacuum or under an argon atmosphere using standard Schlenk techniques unless otherwise specified. All glassware was oven-dried before use. Solvents (pentane, diethyl ether) were distilled under a nitrogen atmosphere from sodium/benzophenone immediately before use. Magnesium turnings (Fisher) were used as received. The compounds $(COD)PtCl_2$,[123] 4-bromo-3,3-dimethyl-1-butene,[124] (2,2-dimethylbut-3-en-1-yl)-lithium,[124] 5-bromo-4,4-dimethyl-1-pentene,[124] and 6-bromo-5,5-dimethyl-1-hexene,[124] were prepared as described elsewhere. Benzene-d_6 and toluene-d_8 were purchased from Cambridge Isotope Laboratories in 1 mL ampoules and used without purification. SilicaFlash®P60 silica gel was purchased from Silicycle.

Elemental analyses were performed by the University of Illinois Microanalytical Laboratory. The FTIR spectra were acquired on a Thermo Nicolet IR200 spectrometer as mineral oil mulls between KBr plates and processed using the OMNIC software package with automatic baseline corrections. Melting points were acquired on a Thomas−Hoover Uni-Melt apparatus in sealed capillaries under an argon atmosphere. The 1D ^1H, ^2H, and ^{13}C NMR data were recorded on a Varian Inova 400 spectrometer at 9.39 T, a Varian Inova 500 spectrometer at 11.74 T, a Varian Inova 600 spectrometer at 14.09 T, or a Bruker Avance III HD spectrometer equipped with a 5 mm BBFO CryoProbe at 11.74 T. The 1D ^1H−^1H NOE data and the ^{195}Pt NMR data were recorded on a Varian Inova 600 spectrometer at 14.09 T. Chemical shifts are reported in δ units (positive shifts to higher frequency) relative to tetramethylsilane (TMS) (^1H, ^{13}C), set by assigning appropriate shifts to residual solvent signals or to an external standard of aqueous 1.0 M K_2PtCl_6 (^{195}Pt) by sample replacement. X-ray crystallographic data were collected by the staff of the G. L. Clark X-ray Laboratory at the University of Illinois. The gas chromatography−mass spectrometry (GC−MS) spectra were collected on a GC−MS system (Agilent Inc, Palo Alto, CA) consisting of an Agilent 7890 gas chromatograph, an Agilent 5975 mass selective detector, and a HP 7683B autosampler by the staff of the Roy J. Carver Biotechnology Center at the University of Illinois. The peaks

https://dx.doi.org/10.1021/acs.chemmater.0c03226
Chem. Mater. 2020, 32, 9316−9334

were evaluated using the AMDIS 2.71 (NIST, Gaithersburg, MD) program and identified with the aid of the libraries NIST08 (NIST, MD) and W8N08 (Palisade Corporation, NY).

Isothermal thermogravimetric analysis (TGA) data were collected on a TA Instruments Q50 TGA system by the staff of the Materials Research Laboratory at the University of Illinois. Dynamic TGA data were collected on a Cahn TherMax 500 TGA instrument. SEM data were collected on a Hitachi S-4800 High Resolution SEM instrument. GI-XRD data were collected on a PANalytical MRD instrument and processed with the JADE software package. XPS data were collected on a PHI 5400 instrument and processed with the CasaXPS software package. Before being analyzed, the films were treated with ozone for 1 min and then sputtered with Ar^+ for 4 min to remove surface carbon contamination arising from atmospheric exposure. Rutherford backscattering spectra were collected on a 3SDH Pelletron instrument. Atomic force microscopy data were collected on a Cypher S AFM microscope. Electrical conductivities were measured by the four-point probe method.

***cis*-Bis(η^1,η^2-2,2-dimethylbut-3-en-1-yl)platinum (2).** To a solution of (COD)$PtCl_2$ (0.28 g, 0.75 mmol) in diethyl ether (20 mL) at −78 °C was added (2,2-dimethylbut-3-en-1-yl)lithium[124] (20 mL of a 0.09 M solution in pentane, 1.8 mmol). The mixture was stirred at −78 °C for 5 h and was allowed to warm to −20 °C over 5 h. The solvents were slowly removed under vacuum, keeping the temperature at −20 °C to prevent vaporization of the product. The residue was extracted with pentane (2 × 20 mL), and the extracts were filtered, combined, cooled to 0 °C, and quenched with H_2O (5 drops). The resulting solution was dried over Na_2SO_4 at 0 °C, cooled to −78 °C, and filtered. The filtrate was evaporated under vacuum at −20 °C to give a brown oil. The product was purified by column chromatography on silica gel with pentane as the eluent (R_f = 0.30). Slow evaporation of the eluate at −20 °C gave the product as a white solid, which melts to form a light yellow liquid at room temperature. Yield: 0.16 g (58%). Anal. calcd for $C_{12}H_{26}Pt$: C, 39.9; H, 6.14. Found: C, 40.3; H, 6.06. Mp ca. −15 °C. $^{195}Pt\{^1H\}$ NMR (129 MHz, C_7D_8, 20 °C): δ −4019 (br, C_s isomer, relative intensity = 1), −4110 (br, C_2 isomer, relative intensity = 2). At room temperature, the C_2 and C_s isomers are exchanging rapidly: ^1H NMR (500 MHz, C_7D_8, 20 °C): δ 4.39 (dd, 2 H, $^3J_{HH}$ = 15.3, 8.8 Hz, $^2J_{PtH}$ = 40.8 Hz, −CH═), 3.67 (d, 2 H, $^3J_{HH}$ = 15.3 Hz, $^2J_{PtH}$ = 38.6 Hz, ═CH_2), 3.46 (d, 2 H, $^3J_{HH}$ = 8.8 Hz, ═CH_2), 1.08 (br, 12 H, 2-Me), 0.87 (br, 4 H, Pt-CH_2). $^{13}C\{^1H\}$ NMR (126 MHz, C_7D_8, 20 °C): δ 99.72 (br, −CH═), 74.69 (s, $^1J_{PtC}$ = 25.3 Hz, ═CH_2), 37.76 (s, $^2J_{PtC}$ = 113.7 Hz, 2-C), 32.59 (s, $^3J_{PtC}$ = 40.6 Hz, 2-Me), 5.51 (s, $^1J_{PtC}$ = 614 Hz, Pt-CH_2).

Separate NMR peaks can be seen for the two isomers at low temperatures: ^1H NMR (500 MHz, C_7D_8, −60 °C): Major isomer: δ 4.39 (dd, 2 H, $^3J_{HH}$ = 15.2, 8.8 Hz, $^2J_{PtH}$ = 39 Hz, −CH═), 3.65 (d, 2 H, $^3J_{HH}$ = 15.2 Hz, $^2J_{PtH}$ = 41 Hz, ═CH_2), 3.51 (d, 2 H, $^3J_{HH}$ = 8.8 Hz, $^2J_{PtH}$ = 19 Hz, ═CH_2), 1.32 (d, 2 H, $^2J_{HH}$ = 10 Hz, $^2J_{PtH}$ = 86 Hz, Pt-CH_2), 1.22 (s, 6 H, 2-Me), 1.07 (s, 6 H, 2-Me), 0.91 (d, 2 H, $^2J_{HH}$ = 10.0 Hz, $^2J_{PtH}$ = 105 Hz, Pt-CH_2). $^{13}C\{^1H\}$ NMR (126 MHz, C_7D_8, 20 °C): δ 97.37 (s, −CH═), 74.76 (s, $^1J_{PtC}$ = 26 Hz, ═CH_2), 37.82 (s, $^2J_{PtC}$ = 112 Hz, 2-C), 32.45 (s, 2-Me, $^3J_{PtC}$ cannot be obtained due to peak overlapping), 32.45 (s, $^3J_{PtC}$ = 48 Hz, 2-Me, $^3J_{PtC}$), 5.46 (s, $^1J_{PtC}$ = 610.0 Hz, 1-CH_2).

Minor isomer: δ ∼4.37 (m, −CH═), 3.78 (d, 2 H, $^3J_{HH}$ = 15.3 Hz, $^2J_{PtH}$ = 36 Hz, ═CH_2), 3.25 (d, 2 H, $^2J_{HH}$ = 8.7 Hz, $^2J_{PtH}$ = 15 Hz, ═CH_2), 1.29 (s, 6 H, 2-Me), ∼1.18 (d, 2 H, $^2J_{HH}$ = 10 Hz, $^2J_{PtH}$ = ∼70 Hz, Pt-CH_2), 1.04 (s, 6 H, 2-Me), 0.78 (d, 2 H, $^2J_{HH}$ = 10 Hz, $^2J_{PtH}$ = 120 Hz, Pt-CH_2). $^{13}C\{^1H\}$ NMR (126 MHz, C_7D_8, 20 °C): δ 100.80 (s, −CH═), 74.93 (s, $^1J_{PtC}$ = 25 Hz, ═CH_2), 37.54 (s, $^2J_{PtC}$ = 115 Hz, 2-C), 32.79 (s, $^3J_{PtC}$ = 56 Hz, 2-Me, $^3J_{PtC}$), 32.50 (s, 2-Me, $^3J_{PtC}$ cannot be obtained due to peak overlapping), 5.00 (s, $^1J_{PtC}$ = 608.0 Hz, 1-CH_2).

Note: 2,2-dimethylbut-3-en-1-yllithium reacts with silicone grease, so Krytox grease must be used in order to obtain appreciable yield for current scale of reaction.[124]

(2,2-Dimethylpent-4-en-1-yl)magnesium Bromide. A 250 mL three-necked flask equipped with a water-cooled reflux condenser was charged with magnesium turnings (4.0 g, 170 mmol), diethyl ether (20 mL), and 1,2-dibromoethane (9 drops). The mixture was heated to reflux for 12 h and then was treated with 5-bromo-4,4-dimethylpent-1-ene (4.25 g, 24.0 mmol) in one portion while still hot. The mixture was heated to reflux for a further 12 h and then was filtered. The solid residue was extracted with diethyl ether (2 × 10 mL), filtering each time. The filtrates were combined to give a light yellow solution, which was used in the next step. Yield: 24 mL of a 0.41 M solution (41%).

***cis*-Bis(η^1,η^2-2,2-dimethylpent-4-en-1-yl)platinum (3).** To a suspension of (COD)$PtCl_2$ (1.50 g, 3.99 mmol) in diethyl ether (20 mL) at 0 °C was added (2,2-dimethylpent-4-en-1-yl)magnesium bromide (23 mL of a 0.41 M solution in diethyl ether; 9.4 mmol) dropwise with vigorous stirring. The mixture was stirred at 0 °C for 2 h and then was warmed to room temperature. The mixture was filtered, and the solid was extracted with diethyl ether (20 mL). The filtrate and the filtered extract were combined and then the solvent was removed under vacuum. The resulting slurry was extracted with pentane (2 × 20 mL). The extracts were filtered, combined, quenched with water (5 drops), and dried over magnesium sulfate. Pentane was removed on a rotary evaporator, and the product was purified by silica gel column chromatography using pentane as the eluent (R_f = 0.57). The removal of the solvent from the eluate gave a light yellow oil. The oil was recrystallized from ethanol (∼0.2 mL) at −20 °C to give the product as a light yellow solid. Yield: 0.99 g (64%). Anal. calcd for $C_{14}H_{26}Pt$: C, 43.2; H, 6.73. Found: C, 42.9; H, 6.56. Mp ∼20 °C. $^{195}Pt\{^1H\}$ NMR (129 MHz, C_7D_8, 20 °C): δ −3777 (s). ^1H NMR (500 MHz, C_7D_8, 20 °C): δ 4.51 (m, 2 H, −CH═), 3.57 (d, 2 H, $^3J_{HH}$ = 14.7 Hz, $^2J_{PtH}$ = 39.6 Hz, ═CH_2), 3.40 (d, 2 H, $^3J_{HH}$ = 8.0 Hz, $^2J_{PtH}$ = 29.5 Hz, ═CH_2), 2.25 (d, $^2J_{HH}$ = 11.8 Hz, $^2J_{PtH}$ = 36.6 Hz, 2 H, Pt-CH_2 equatorial), 1.91 (dd, $^2J_{HH}$ = 11.4 Hz, $^3J_{HH}$ = 4.2 Hz, 2 H, 3-CH_2 equatorial), 1.64 (d, $^2J_{HH}$ = 11.7 Hz, $^2J_{PtH}$ = 102.9 Hz, 2H, Pt-CH_2 axial), 1.47 (dd, $^2J_{HH}$ = 11.4 Hz, $^3J_{HH}$ = 9.6 Hz, 2 H, 3-CH_2 axial), 1.24 (s, 6 H, 2-Me axial), 1.13 (s, 6 H, $^4J_{PtH}$ = 9.9 Hz, 2-Me equatorial). $^{13}C\{^1H\}$ NMR (126 MHz, C_7D_8, 20 °C): δ 104.67 (s, $^1J_{PtC}$ = 16 Hz, −CH═), 88.76 (s, $^1J_{PtC}$ = 29.4 Hz, ═CH_2), 51.14 (s, 2-C), 48.69 (s, 3-CH_2), 43.30 (s, $^1J_{PtC}$ = 843.6 Hz, 1-CH_2), 33.08 (s, $^3J_{PtC}$ = 99.6 Hz, 2-Me equatorial), 31.99 (s, $^3J_{PtC}$ = 32.3 Hz, 2-Me axial).

***cis*-Bis(η^1,η^2-2,2-dimethylhex-5-en-1-yl)platinum (4).** This compound was prepared from 6-bromo-5,5-dimethyl-1-hexene via the Grignard reagent according to the procedure for synthesizing *cis*-bis(η^1,η^2-2,2-dimethylpent-4-en-1-yl)platinum. After being purified by column chromatography using pentane as the eluent (R_f = 0.50), it was further purified by slow evaporation of pentane from an ethanol/pentane solution at −78 °C. The resulting thermally sensitive yellow crystals were collected and dried. Yield: 51 mg (10%). Anal. calcd for $C_{16}H_{30}Pt$: C, 46.0; H, 7.24. Found: C, 46.2; H, 6.91. Mp 46−47 °C. $^{195}Pt\{^1H\}$ NMR (129 MHz, C_7D_8, 20 °C): δ −3778 (s, C_s isomer, relative intensity =1), -3797 (s, C_2 isomer, relative intensity = 5). ^1H NMR (500 MHz, C_7D_8, 20 °C): Major isomer: δ 4.28 (d, 2 H, $^3J_{HH}$ = 15 Hz, ═CH_2), 4.14 (m, 2 H, −CH═), 3.39 (d, 2 H, $^3J_{HH}$ = 9.1 Hz, $^2J_{PtH}$ = 34.2 Hz, ═CH_2), 2.30 (d, $^2J_{HH}$ = 9.3 Hz, $^2J_{PtH}$ = 64 Hz, 2 H, Pt-CH_2 equatorial), 2.14 (m, 2 H, 4-CH_2), 1.80 (d, $^2J_{HH}$ = 7 Hz, $^2J_{PtH}$ = 105 Hz, 2H, Pt-CH_2 axial), 1.55−1.75 (m, 4 H, 3-CH_2 & 4-CH_2), 1.20 (br, 2H, 3-CH_2), 1.15 (br, 6 H, 2-Me equatorial), 1.00 (br, 6 H, 2-Me axial). $^{13}C\{^1H\}$ NMR (151 MHz, C_7D_8, 20 °C): δ 104.51 (br, −CH═), 82.86 (br, ═CH_2), 46.66 (s, $^1J_{PtC}$ = 860.9 Hz, Pt-CH_2), 40.07 (br, 2-C), 37.72 (s, $^3J_{PtC}$ = 97 Hz, 2-Me equatorial), 37.33 (br, $^3J_{PtC}$ = 20 Hz, 3-CH_2), 28.86 (br, 2-Me axial), 28.05 (br, 4-CH_2).

Minor isomer is not observable at room temperature, but a second set of peaks are clearly shown in the ^{13}C NMR spectrum in toluene-d_8 at −30 °C (Figure S4.16). Major isomer: $^{13}C\{^1H\}$ NMR (151 MHz, C_7D_8, −30 °C): δ 104.06 (br, −CH═), 82.48 (br, ═CH_2), 46.64 (s, $^1J_{PtC}$ = 853.85 Hz, Pt-CH_2), 40.12 (br, $^2J_{PtC}$ = 38.82 Hz, 2-C), 37.87 (s, $^3J_{PtC}$ = 98.16 Hz, 2-Me equatorial), 36.78 (br, $^3J_{PtC}$ = 20 Hz, 3-CH_2), 28.73 (br, 2-Me axial), 27.91 (br, 4-CH_2, J_{PtC} = 14.15 Hz). Minor isomer: $^{13}C\{^1H\}$ NMR (151 MHz, C_7D_8, −30 °C): δ 106.27 (br, −CH═), 81.36 (br, ═CH_2), 47.28 (s, Pt-CH_2). Other

https://dx.doi.org/10.1021/acs.chemmater.0c03226
Chem. Mater. 2020, 32, 9316−9334

resonances cannot be unambiguously identified due to peak overlapping.

General Crystallographic Procedure. The following details were common to all of the crystal structure determinations; for details about individual compounds, see Supporting Information, Section S3. Crystals mounted on glass fibers with either Krytox or Paratone oil were transferred onto the diffractometer and kept at −173 °C in a cold nitrogen gas stream. Intensity data were collected on a Bruker Apex II diffractometer equipped with a CCD detector or a Bruker D8 Venture kappa diffractometer equipped with a Photon 100 CMOS detector. Standard peak search and indexing procedures gave rough cell dimensions. Data were collected with an area detector using the measurement parameters listed in Table 1. The measured intensities were reduced to structure factor amplitudes and their estimated standard deviations by correction for background, scan speed, and Lorentz and polarization effects. No corrections for crystal decay were necessary. Systematically absent reflections were deleted and symmetry equivalent reflections were averaged to yield the set of unique data. The structure was solved by direct methods (SHELXTL); subsequent least-squares refinement and difference Fourier calculations revealed the positions of all of the non-hydrogen atoms and the olefinic hydrogen atoms (for **2**, **3**, and **4**) on the ω-alkenyl ligands. The analytical approximations to the scattering factors were used, and all structure factors were corrected for both real and imaginary components of anomalous dispersion. The methyl groups were allowed to rotate about the C−C axis to find the best least-squares positions. The displacement parameters for methylene and methine hydrogens were set equal to 1.2 times U_{eq} for the attached carbon; those for methyl hydrogens were set to 1.5 times U_{eq}. In the final cycle of least-squares, independent anisotropic displacement factors were refined for the non-hydrogen atoms. Final refinement parameters are given in Table 1. A final analysis of variance between the observed and calculated structure factors showed no apparent errors.

^{1}H{^{1}H} NOE Spectra of *cis*-Bis(η^1,η^2-2,2-dimethylpent-4-en-1-yl)platinum (3). The 1D ^{1}H{^{1}H} NOE NMR spectra of **3** were measured at −20 °C by means of a NOESY 1D experiment with a 500 ms mixing time. At this temperature, the olefin face exchange rate for the Pt−olefin interaction is slow. The NOE results confirm the assignments made on the basis of the magnitudes of the Pt−H coupling constants. Thus, when the axial Pt-CH_2 resonance at δ 1.59 was irradiated, sizable NOE signals are seen for the resonances at δ 2.21 and at δ 1.19, which are assigned to the equatorial Pt-CH_2 resonance and the equatorial 2-Me resonances, respectively (Figure S4.7). When the equatorial Pt-CH_2 resonance at δ 2.21 was irradiated, both methyl resonances show sizable NOEs. When the equatorial γ-CH_2 resonance at δ 1.89 was irradiated, the olefinic methine peak and both methyl peaks show sizable NOEs.

Variable Temperature ^{1}H NMR Spectra and NMR Simulations. Simulations of variable temperature NMR line shapes to determine the olefin face exchange rates were performed with the program WINDNMR.[85] Before the simulations were performed, the experimental spectra were phased and baseline-corrected using the NUTS software package (Acorn NMR Inc.).[125] The chemical shift difference between the slow-exchange resonances is linearly dependent on temperature, and we assumed that the low-temperature trend in the difference could be extrapolated to temperatures above the coalescence point. The rates of exchange as a function of temperature were determined from visual comparisons of the experimental spectra with computed trial line shapes. At each temperature, the exchange rate was the value that gave the best fit of the calculated to the observed line shape. For a two-site exchange, the WINDNMR package parameterizes the "rate" of exchange as the sum of the forward and backward rate constants ($k_{ab} + k_{ba}$).[126] For a first-order exchange between two sites of equal population, the actual rate constant (i.e., either k_{ab} or k_{ba}) is half of this parameter. For a first-order exchange between two sites of unequal population, the actual rate constants are given by k_{ab} (i.e., leaving the a site) = (mole fraction of the b site)($k_{ab} + k_{ba}$) and similarly for k_{ba}.

Activation parameters were determined by fitting the rates as a function of temperature to the Eyring equation. The errors in the rate constants of ca. 20% were estimated on the basis of subjective judgments of the sensitivities of the fits to changes in the rate constants. The temperature of the NMR probe was calibrated using a methanol temperature standard,[127] and the estimated error in the temperature measurements was 1 K. Uncertainties in the activation parameters were estimated from propagation of error formulae.[128]

For the pentenyl compound **3**, the ^{1}H NMR spectra were collected in toluene-d_8 at 24 temperatures between 11 and 69 °C. The ^{1}H NMR line shapes of the resonances due to the diastereotopic β-Me groups were simulated to extract the olefin face exchange rate. The natural linewidth (FWHM = 2.6 Hz) was measured from the resonance for the axial methyl group at −22 °C, a temperature at which the exchange is in the slow-exchange limit. Because the equatorial methyl resonance shows significant ^{195}Pt−^{1}H coupling, the exchange rates in the slow-exchange regime (11−36 °C) were determined by fitting the line shape of only the axial methyl resonance. Above 36 °C, as coalescence is approached, the equatorial methyl resonance is sufficiently broad that the ^{195}Pt satellites are no longer evident, but we found that we could successfully simulate the line shapes in this temperature range by assigning the equatorial methyl resonance an effective natural linewidth (FWHM) of 4.0 Hz.

For the butenyl and hexenyl compounds **2** and **4**, analyses of the variable temperature ^{1}H NMR spectra are made more difficult by two factors: both compounds exist in solution as a mixture of two isomers and the peaks suffered from overlapping and coupling to ^{195}Pt. We found that it was far easier to simulate the variable temperature ^{13}C{^{1}H} NMR line shapes for exchange between the C_2 and C_s isomers. For **2** and **4**, most of the ^{13}C{^{1}H} NMR resonances show ^{195}Pt−^{13}C coupling, but because couplings to the α-carbon resonances for the C_2 and C_s isomers are so large ($^1J_{PtC}$ ∼600 Hz for **2** and ∼800 Hz for **4**), the line shapes of the central features of these resonances are well separated from (and unaffected by overlap with) their ^{195}Pt satellites. In addition, for **2**, we also studied the olefinic methine carbon resonances of the C_2 and C_s isomers, which show no ^{195}Pt−^{13}C coupling.

For **2**, the natural line widths of the ^{13}C{^{1}H} NMR resonances (FWHM = 1.6 Hz for the C_s isomer and 2.2 Hz for the C_2 isomer) were taken from the ^{13}C{^{1}H} NMR spectrum at −62 °C, which is at the slow-exchange limit. For **4**, the slow-exchange natural linewidth of the ^{13}C{^{1}H} NMR resonances (FWHM = 2.3 Hz) for the C_s isomer was taken from the ^{13}C{^{1}H} NMR spectrum at −21 °C. Because the resonance for the C_2 isomer at −21 °C is broad (probably due to slowing of ring conformational motion), the slow-exchange natural line widths (FWHM = 2.4 Hz) for the C_2 isomer were extrapolated from the linewidth seen in the ^{13}C{^{1}H} NMR spectrum at −8 °C by assuming that this resonance narrows at a lower temperature in the same way as does the C_s isomer. The equilibrium constant $K = [C_2]/[C_s]$ was measured by ^{1}H NMR spectroscopy over temperatures (−83 to −41 °C for **2**, −83 to 21 °C for **4**) at which the two isomers are slowly exchanging; the activation parameters obtained from a van't Hoff plot were used to extrapolate this equilibrium constant to higher temperatures (Figure S6.2 and S6.14), and the resulting mole fractions were used in the simulations.

For **3**, the rate measured based on the line broadening of the methyl resonances is actually the rate of converting one enantiomer of the C_2 isomer to the other. The rate of interest (olefin decomplexation) corresponds to the rate of conversion of the C_2 isomer to the C_s isomer, which based on the scheme below should be twice of the rate of the interconversion between the C_2 isomers, because each time a C_2 isomer is converted to a C_s isomer, it converts to its enantiomer with a probability of 50%. Because the rate of decomplexation is twice the measured rate, the entropy of activation of decomplexation should be ∼1 eu larger than the value obtained by fitting the measured rate to the Eyring equation.

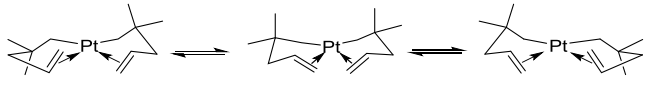

https://dx.doi.org/10.1021/acs.chemmater.0c03226
Chem. Mater. 2020, 32, 9316−9334

Volatility of *cis*-Bis(η^1,η^2-2,2-dimethylpent-4-en-1-yl)platinum (3). The vapor pressure and molar enthalpy of sublimation of **3** were measured from the isothermal evaporation rates by means of the following equation, which is a modified version of the Langmuir equation for free evaporation in vacuum:[129]

$$p = k(\mathrm{d}m/\mathrm{d}t)\sqrt{T/M}$$

where p is the vapor pressure, $\mathrm{d}m/\mathrm{d}t$ is the mass loss rate, T is the absolute temperature, and M is the molecular weight. The parameter k is an instrument-specific factor that depends in a complex way on the experimental conditions used to carry out the isothermal measurements; its value can be determined by measuring the isothermal evaporation rate of a calibration standard at different temperatures and comparing the evaporation rate with the reported vapor pressure at each temperature. Because **3** liquefies with gentle heating, 1-methylnaphthalene (which is also a liquid at room temperature) was chosen as the standard; from its reported temperature-dependent vapor pressure[130] and evaporation experiments conducted on our instrument, we found that the parameter k has a value of 5.4×10^{-3} Torr $K^{1/2}$ $g^{3/2}$ $mol^{1/2}$ min^{1}.

The isothermal evaporation rate of **3** was measured on the same instrument with the same purge gas flow rate, and from the calibration we determined the vapor pressure as a function of temperature. A fit of the data to the August equation[131] gives $\log p = 6.19 - 2400/T$ (pressure is in Torr and temperature is in K). For example, the vapor pressure of **3** is 10 mTorr at 20 °C and 250 mTorr at 80 °C. The vapor pressure of **3** at 80 °C is higher than the 45 mTorr vapor pressure reported for the related platinum(II) dialkyl diolefin complex (COD)$PtMe_2$.[20]

The molar enthalpy of sublimation ΔH_{vap} was determined to be 11 ± 2 kcal mol^{-1} from a fit of $\ln p$ to $1/T$ according to the Clausius–Clapeyron equation

$$\ln p = B - \frac{\Delta H_{vap}}{RT}$$

where B is a constant. The enthalpy of evaporation of **3** is similar to that of 10.5 ± 0.3 kcal mol^{-1} for the commercial precursor (C_5H_4Me)$PtMe_3$.[7]

Cold Wall CVD Experiments. CVD experiments were performed in a cold wall high-vacuum chamber described elsewhere.[99,100] The precursor was loaded into a glass reservoir, which was kept at 75 °C during deposition experiments. A flow rate of 20–30 sccm argon (99.999%) was used as a carrier; the precursor was delivered into the chamber through a 0.4 cm i.d. stainless steel tube pointing toward the substrate. The total chamber pressure (Ar and precursor, measured by the manometer attached to the chamber) was kept at 2 to 3 mTorr. A remote microwave plasma source consisting of a 9.5 mm i.d. Pyrex tube with a 2.45 GHz Evenson cavity located outside of the chamber[132] was used to generate atomic oxygen from research grade dioxygen gas (99.999%). For these experiments, the flow of O_2 was regulated with a mass flow controller to establish a partial pressure in the chamber of 1.5 mTorr. The net plasma power (forward minus reflected) was 70 W.

Several different substrates were tested. 10 nm films of Al_2O_3 were grown on Si (100) by ALD from trimethylaluminum and water at 80 °C. Vanadium nitride (VN) was grown by in situ CVD from tetrakis(dimethylamido)vanadium and ammonia at 330 °C on Si (100). Silicon (Si(100) with native oxide) and Al_2O_3 substrates were cleaned by UV/ozone to remove ambient contaminations for 10 min before loading into the chamber. All substrates were radiatively heated. The temperatures were measured with a K-type thermocouple attached to the sample holder.

The onset of nucleation was monitored by real-time spectroscopic ellipsometry (SE), and the changes in the angle Ψ were reported at a single energy, 2.65 eV, which provides the greatest sensitivity to the onset of nucleation, as discussed previously.[101] Film thickness was measured by scanning electron microscopy (Hitachi 4800) and Rutherford backscattering spectroscopy, RBS (3SDH Pelletron). The film growth rates were calculated by dividing the RBS thickness by the growth time. The carbon content in the films was measured by RBS. Surface roughness was measured by atomic force microscopy (Asylum Research Cypher) using a silicon nitride cantilever in contact mode.

Thermolysis of 3 in the Condensed State. The thermolysis of **3** in the condensed state begins at ∼145 °C and is largely complete by 175 °C, as judged by thermogravimetric analysis under an atmosphere of N_2. The final mass after pyrolysis is 45% of the original mass; for comparison, 50% of the mass of **3** is Pt.

The ∼5% mass loss seen during the ∼10 min ramp to 120 °C (Figure S7.5) is not due to thermolysis of **3** but can be ascribed to a small amount of vaporization; thermolysis of **3** in C_6D_6 follows a unimolecular decomposition mechanism with a first-order rate constant of 9×10^{-4} min^{-1} at 120 °C,[133] and at this rate it would take much longer (∼60 min) for ∼5% of **3** to decompose at this temperature.

We estimate that it will take ∼400 h at 75 °C and ∼200 h at 80 °C for 5% of **3** to decompose.

Thermolysis of 3 under Static Vacuum CVD Conditions. To collect and analyze quantitatively the gaseous products generated under CVD conditions, **3** was thermolyzed under static vacuum (10 mTorr) in a previously described glass apparatus.[107,134] This apparatus consisted of a solvent reservoir, a precursor reservoir, a vertical deposition zone, and an NMR tube. The apparatus was modified from the previous design by placing four indentations in the vertical hot zone so that a substrate could be coated during thermolysis and subsequently analyzed to assess the film properties. The hot zone was heated with heating tape and the temperature was regulated with a variable transformer. Temperatures were measured with a K-type thermocouple held next to the hot zone under the heating tape. The residual protons of commercial C_6D_6 (99.5%) were used as an integration standard. The concentration of protons in this solvent (0.284 mmol g^{-1}) was assessed by dissolving 1,2,4,5-tetrachlorobenzene (32.7 mg, 0.151 mmol) in the C_6D_6 solvent (0.959 g) and measuring the relative intensity of the ^1H NMR signals, employing a 150 s post-acquisition delay to eliminate integration errors due to long relaxation times for the aromatic protons.

The solvent reservoir was charged with C_6D_6 (0.850 g), which was degassed with 3 freeze–pump–thaw cycles; the solvent reservoir was isolated from the rest of the apparatus until the deposition step was complete. Because **3** is low melting, it is difficult to load into the apparatus as the pure material. As a result, **3** (69.0 mg, 0.177 mmol) was dissolved in pentane (5 mL) and the solution was transferred into the precursor reservoir with a syringe. The pentane solvent was carefully removed at 0 °C, a temperature at which the evaporation of precursor is negligible. CVD growth was conducted at 250 ± 10 °C, with the precursor reservoir maintained at 80 °C.

Byproducts from the thermolysis were trapped in the NMR tube, which was cooled with liquid nitrogen. After the deposition was complete, the known amount of C_6D_6 solvent was transferred into the NMR tube.[107,134] As judged from quantitation of the contents of the NMR tube, all (105 ± 10%) of the protons in the precursor were accounted for in the byproducts collected in the NMR tube, indicating that all of the volatile products had been trapped. The identities of the products were determined from their ^1H, COSY, and HSQC NMR spectra and GC–MS data (Figure S10.1–S10.9).

■ ASSOCIATED CONTENT

Supporting Information

The Supporting Information is available free of charge at https://pubs.acs.org/doi/10.1021/acs.chemmater.0c03226.

Crystallographic data (CIF)
Crystallographic data (CIF)
Crystallographic data (CIF)
Crystallographic data (CIF)
Crystallographic data (CIF)
Syntheses and characterization of bromo(2,2-dimethylbut-3-en-1-yl)(1,5-cyclooctadiene)platinum (**5**), bis(η^1-2,2-dimethylbut-3-en-1-yl)(1,5-cyclooctadiene)platinum

https://dx.doi.org/10.1021/acs.chemmater.0c03226
Chem. Mater. 2020, 32, 9316–9334

(6), and bis[η^1-(2,2-dimethylcyclopentyl)methyl](1,5-cyclooctadiene)platinum (7); details of crystallography characterizations; ^{1}H, ^{13}C, ^{195}Pt, HSQC NMR, IR, and UV/vis spectra of bis(η^1,η^2-2,2-dimethyl-ω-alkenyl)-platinum compounds **2**, **3**, and **4**; ^{1}H and ^{13}C VT-NMR spectra, NMR line shape fits, and Eyring plot of bis(η^1,η^2-2,2-dimethyl-ω-alkenyl)platinum compounds, and van't Hoff plot of the C_2 and C_s isomers of **2** and **4**; measured vapor pressure of **3** at different temperatures and related plots; film characterization data, including the film growth rate, Arrhenius plot, SEM images, RBS spectra, and glancing angle (1°) XRD spectra of the films grown in the cold wall apparatus; film characterization data, SEM image, XPS spectra, and glancing angle (1°) XRD spectra of the films grown in the hot wall apparatus; ^{1}H, COSY, HSQC NMR, and GC−MS spectra of the thermolysis products generated in the static vacuum CVD apparatus, with the assignment of each species; spectroscopic evidence showing that **3** does not react with H_2 (PDF)

AUTHOR INFORMATION

Corresponding Author

Gregory S. Girolami − *School of Chemical Sciences, University of Illinois at Urbana-Champaign, Urbana, Illinois 61801, United States;* orcid.org/0000-0002-7295-1775; Email: girolami@scs.illinois.edu

Authors

Sumeng Liu − *School of Chemical Sciences, University of Illinois at Urbana-Champaign, Urbana, Illinois 61801, United States;* orcid.org/0000-0002-2133-2122

Zhejun Zhang − *Department of Materials Science and Engineering, University of Illinois at Urbana-Champaign, Urbana, Illinois 61801, United States*

Danielle Gray − *School of Chemical Sciences, University of Illinois at Urbana-Champaign, Urbana, Illinois 61801, United States;* orcid.org/0000-0003-0059-2096

Lingyang Zhu − *School of Chemical Sciences, University of Illinois at Urbana-Champaign, Urbana, Illinois 61801, United States;* orcid.org/0000-0002-6657-271X

John R. Abelson − *Department of Materials Science and Engineering, University of Illinois at Urbana-Champaign, Urbana, Illinois 61801, United States*

Complete contact information is available at: https://pubs.acs.org/10.1021/acs.chemmater.0c03226

Author Contributions

All authors have given approval to the final version of the manuscript.

Notes

The authors declare the following competing financial interest(s): One patent related to this work has been filed: Metal Complexes for Depositing Films and Method of Making and Using the Same, U.S. Patent 20190077819 (Published Mar. 14th, 2019).

ACKNOWLEDGMENTS

We thank the National Science Foundation under grants CHE 1665191 and CHE 1954745 (to G.S.G.) and CMMI 1825938 (to J.R.A.) for support of this research.

REFERENCES

(1) Gozum, J. E.; Pollina, D. M.; Jensen, J. A.; Girolami, G. S. "Tailored" Organometallics as Precursors for the Chemical Vapor Deposition of High-Purity Palladium and Platinum Thin Films. *J. Am. Chem. Soc.* **1988**, *110*, 2688−2689.

(2) Doppelt, P. Why is Coordination Chemistry Stretching the Limits of Micro-Electronics Technology? *Coord. Chem. Rev.* **1998**, *178−180*, 1785−1809.

(3) Hampden-Smith, M. J.; Kodas, T. T. Chemical Vapor Deposition of Metals: Part 1. An Overview of CVD Processes. *Chem. Vap. Depos.* **1995**, *1*, 8−23.

(4) Jones, A. C.; Hitchman, M. L. Overview of Chemical Vapour Deposition. In *Chemical Vapour Deposition: Precursors, Processes and Applications*; Jones, A. C.; Hitchman, M. L., Eds.; The Royal Society of Chemistry: Cambridge, 2009; pp 1−36.

(5) Mackus, A. J. M.; Leick, N.; Baker, L.; Kessels, W. M. M. Catalytic Combustion and Dehydrogenation Reactions during Atomic Layer Deposition of Platinum. *Chem. Mater.* **2012**, *24*, 1752−1761.

(6) Xue, Z.; Strouse, M. J.; Shuh, D. K.; Knobler, C. B.; Kaesz, H. D.; Hicks, R. F.; Williams, R. S. Characterization of (Methylcyclopentadienyl)trimethylplatinum and Low-Temperature Organometallic Chemical Vapor Deposition of Platinum Metal. *J. Am. Chem. Soc.* **1989**, *111*, 8779−8784.

(7) Xue, Z.; Thridandam, H.; Kaesz, H. D.; Hicks, R. F. Organometallic Chemical Vapor Deposition of Platinum. Reaction Kinetics and Vapor Pressures of Precursors. *Chem. Mater.* **1992**, *4*, 162−166.

(8) Hiratani, M.; Nabatame, T.; Matsui, Y.; Imagawa, K.; Kimura, S. Platinum Film Growth by Chemical Vapor Deposition Based on Autocatalytic Oxidative Decomposition. *J. Electrochem. Soc.* **2001**, *148*, C524−C527.

(9) Knoops, H. C. M.; Mackus, A. J. M.; Donders, M. E.; van de Sanden, M. C. M.; Notten, P. H. L.; Kessels, W. M. M. Remote Plasma ALD of Platinum and Platinum Oxide Films. *Electrochem. Solid-State Lett* **2009**, *12*, G34−G36.

(10) Dryden, N. H.; Kumar, R.; Ou, E.; Rashidi, M.; Roy, S.; Norton, P. R.; Puddephatt, R. J.; Scott, J. D. Chemical Vapor Deposition of Platinum: New Precursors and Their Properties. *Chem. Mater.* **1991**, *3*, 677−685.

(11) Dendooven, J.; Ramachandran, R. K.; Devloo-Casier, K.; Rampelberg, G.; Filez, M.; Poelman, H.; Marin, G. B.; Fonda, E.; Detavernier, C. Low-Temperature Atomic Layer Deposition of Platinum Using (Methylcyclopentadienyl)trimethylplatinum and Ozone. *J. Phys. Chem. C* **2013**, *117*, 20557−20561.

(12) Pierson, H. O. Introduction and General Considerations. In *Handbook of Chemical Vapor Deposition*; Pierson, H. O., Ed.; William Andrew Publishing: Oxford, 1992; pp 1−16.

(13) Green, M. L.; Levy, R. A. Chemical Vapor Deposition of Metals for Integrated Circuit Applications. *JOM* **1985**, *37*, 63−71.

(14) Hämäläinen, J.; Ritala, M.; Leskelä, M. Atomic Layer Deposition of Noble Metals and Their Oxides. *Chem. Mater.* **2014**, *26*, 786−801.

(15) George, S. M. Atomic Layer Deposition: An Overview. *Chem. Rev.* **2010**, *110*, 111−131.

(16) Bernal Ramos, K.; Saly, M. J.; Chabal, Y. J. Precursor Design and Reaction Mechanisms for the Atomic Layer Deposition of Metal Films. *Coord. Chem. Rev.* **2013**, *257*, 3271−3281.

(17) Aaltonen, T.; Ritala, M.; Sajavaara, T.; Keinonen, J.; Leskelä, M. Atomic Layer Deposition of Platinum Thin Films. *Chem. Mater.* **2003**, *15*, 1924−1928.

(18) Fang, Q.; Hodson, C.; Xu, C.; Gunn, R. Nucleation and Growth of Platinum Films on High-k/Metal Gate Materials by Remote Plasma and Thermal ALD. *Phys. Procedia* **2012**, *32*, 551−560.

(19) Baum, T. H.; Comita, P. B. Laser-Induced Chemical Vapor Deposition of Metals for Microelectronics Technology. *Thin Solid Films* **1992**, *218*, 80−94.

(20) Hierso, J.-C.; Serp, P.; Feurer, R.; Kalck, P. MOCVD of Rhodium, Palladium and Platinum Complexes on Fluidized Divided

Substrates: Novel Process for One-Step Preparation of Noble-Metal Catalysts. *Appl. Organomet. Chem.* **1998**, *12*, 161−172.
(21) Dossi, C.; Psaro, R.; Bartsch, A.; Fusi, A.; Sordelli, L.; Ugo, R.; Bellatreccia, M.; Zanoni, R.; Vlaic, G. Chemical Vapor Deposition of Platinum Hexafluoroacetylacetonate Inside KL Zeolite: A New Route to Nonacidic Platinum-in-Zeolite Catalysts. *J. Catal.* **1994**, *145*, 377−383.
(22) Serp, P.; Kalck, P.; Feurer, R. Chemical Vapor Deposition Methods for the Controlled Preparation of Supported Catalytic Materials. *Chem. Rev.* **2002**, *102*, 3085−3128.
(23) Choi, D. S.; Robertson, A. W.; Warner, J. H.; Kim, S. O.; Kim, H. Low-Temperature Chemical Vapor Deposition Synthesis of Pt−Co Alloyed Nanoparticles with Enhanced Oxygen Reduction Reaction Catalysis. *Adv. Mater.* **2016**, *28*, 7115−7122.
(24) Ryan, M. Platinum in Next-Generation Materials for Data Storage. *Platinum Metals Rev.* **2010**, *54*, 244−249.
(25) Dorovskikh, S. I.; Zharkova, G. I.; Turgambaeva, A. E.; Krisyuk, V. V.; Morozova, N. B. Chemical Vapour Deposition of Platinum Films on Electrodes for Pacemakers: Novel Precursors and Their Thermal Properties. *Appl. Organomet. Chem.* **2016**, *31*, No. e3654.
(26) Woodward, B. K. Platinum Group Metals (PGMs) for Permanent Implantable Electronic Devices. In *Metals for Biomedical Applications*; Baltzer, N.; Copponnex, T., Eds.; Woodhead Publishing: Sawston, Cambridge, 2014; pp 130−147.
(27) Morcos, B. M.; O'Callaghan, J. M.; Amira, M. F.; Van Hoof, C.; Op de Beeck, M. Electrodeposition of Platinum Thin Films as Interconnects Material for Implantable Medical Applications. *J. Electrochem. Soc.* **2013**, *160*, D300−D306.
(28) Baker, L.; Cavanagh, A. S.; Seghete, D.; George, S. M.; Mackus, A. J. M.; Kessels, W. M. M.; Liu, Z. Y.; Wagner, F. T. Nucleation and Growth of Pt Atomic Layer Deposition on Al_2O_3 Substrates Using (Methylcyclopentadienyl)-trimethyl Platinum and O_2 Plasma. *J. Appl. Phys.* **2011**, *109*, No. 084333.
(29) Mackus, A. J. M.; Verheijen, M. A.; Leick, N.; Bol, A. A.; Kessels, W. M. M. Influence of Oxygen Exposure on the Nucleation of Platinum Atomic Layer Deposition: Consequences for Film Growth, Nanopatterning, and Nanoparticle Synthesis. *Chem. Mater.* **2013**, *25*, 1905−1911.
(30) Lien, C.; Konh, M.; Chen, B.; Teplyakov, A. V.; Zaera, F. Gas-Phase Electron-Impact Activation of Atomic Layer Deposition (ALD) Precursors: $MeCpPtMe_3$. *J. Phys. Chem. Lett.* **2018**, *9*, 4602−4606.
(31) Erkens, I. J. M.; Verheijen, M. A.; Knoops, H. C. M.; Keuning, W.; Roozeboom, F.; Kessels, W. M. M. Plasma-Assisted Atomic Layer Deposition of Conformal Pt Films in High Aspect Ratio Trenches. *J. Chem. Phys.* **2016**, *146*, No. 052818.
(32) Elam, J. W.; Zinovev, A. V. V.; Pellin, M. J.; Comstock, D. J.; Hersam, M. C. Nucleation and Growth of Noble Metals on Oxide Surfaces Using Atomic Layer Deposition. *ECS Trans.* **2007**, *3*, 271−278.
(33) Elliott, S. D. Mechanism, Products, and Growth Rate of Atomic Layer Deposition of Noble Metals. *Langmuir* **2010**, *26*, 9179−9182.
(34) Chen, Y. J.; Kaesz, H. D.; Thridandam, H.; Hicks, R. F. Low-Temperature Organometallic Chemical Vapor Deposition of Platinum. *Appl. Phys. Lett.* **1988**, *53*, 1591−1592.
(35) Tagge, C. D.; Simpson, R. D.; Bergman, R. G.; Hostetler, M. J.; Girolami, G. S.; Nuzzo, R. G. Synthesis of a Novel Volatile Platinum Complex for Use in CVD and a Study of the Mechanism of Its Thermal Decomposition in Solution. *J. Am. Chem. Soc.* **1996**, *118*, 2634−2643.
(36) Malandrino, G.; Nigro, R. L.; Fragalà, I. L. MOCVD of Platinum (100) Films on Random Hastelloy C276. *Chem. Vap. Depos.* **1999**, *5*, 59−61.
(37) Shibutami, T.; Kawano, K.; Oshima, N.; Yokoyama, S.; Funakubo, H. Ruthenium Film with High Nuclear Density Deposited by MOCVD Using a Novel Liquid Precursor. *Electrochem. Solid-State Lett.* **2003**, *6*, C117−C119.
(38) Lee, W.-J.; Wan, Z.; Kim, C.-M.; Oh, I.-K.; Harada, R.; Suzuki, K.; Choi, E.-A.; Kwon, S.-H. Atomic Layer Deposition of Pt Thin Films Using Dimethyl (*N*,*N*-Dimethyl-3-Butene-1-Amine-*N*) Platinum and O_2 Reactant. *Chem. Mater.* **2019**, *31*, 5056−5064.
(39) Jiang, M.; Zhang, M.; Li, C.; Williams, C. T.; Liang, C. CVD of $Pt(C_5H_9)_2$ to Synthesize Highly Dispersed Pt/SBA-15 Catalysts for Hydrogenation of Chloronitrobenzene. *Chem. Vap. Depos.* **2014**, *20*, 146−151.
(40) Foley, P.; DiCosimo, R.; Whitesides, G. M. Mechanism of Thermal Decomposition of Dineopentylbis(triethylphosphine)-platinum(II): Formation of Bis(triethylphosphine)-3,3-dimethylplatinacyclobutane. *J. Am. Chem. Soc.* **1980**, *102*, 6713−6725.
(41) Brainard, R. L.; Miller, T. M.; Whitesides, G. M. Mechanisms of Thermal Decomposition of *trans*-Chloroneopentylbis-(tricyclopentylphosphine)platinum(II). *Organometallics* **1986**, *5*, 1481−1490.
(42) DiCosimo, R.; Moore, S. S.; Sowinski, A. F.; Whitesides, G. M. Cyclometalation of Dialkylbis(triethylphosphine)platinum(II) Complexes: Formation of *Pt,Pt*-Bis(triethylphosphine)platinacycloalkanes. *J. Am. Chem. Soc.* **1982**, *104*, 124−133.
(43) Wilkinson, G. The Transition Metal to Carbon Sigma Bond. *Pure Appl. Chem.* **1972**, *30*, 627−636.
(44) Collier, M. R.; Lappert, M. F.; Truelock, M. M. μ-Methylene Transition Metal Binuclear Compounds: Complexes with Me_3SiCH_2- and Related Ligands. *J. Organomet. Chem.* **1970**, *25*, C36−C38.
(45) Wilkinson, G. The Long Search for Stable Transition Metal Alkyls. *Science* **1974**, *185*, 109.
(46) Yagupsky, G.; Mowat, W.; Shortland, A.; Wilkinson, G. Trimethylsilylmethyl Compounds of Transition Metals. *J. Chem. Soc. D* **1970**, 1369−1370.
(47) Lehmkuhl, H.; Naydowski, C.; Benn, R.; Rufińska, A.; Schroth, G.; Mynott, R.; Krüger, C. η^1,η^2-4-Alkenyl(η^5-cyclopentadienyl)-nickel-Komplexe. *Chem. Ber.* **1983**, *116*, 2447−2465.
(48) Richey, H. G.; Rees, T. C. Facile Intramolecular Cyclization of an Olefinic Grignard Reagent. *Tetrahedron Lett* **1966**, *7*, 4297−4301.
(49) Fantasia, S.; Jacobsen, H.; Cavallo, L.; Nolan, S. P. Insertion of a N-Heterocyclic Carbene (NHC) into a Platinum-Olefin Bond. *Organometallics* **2007**, *26*, 3286−3288.
(50) Da, T. T.; Hong Hai, L. T.; Meervelt, L. V.; Dinh, N. H. Synthesis, Structure, and in vitro Cytotoxicity of Organoplatinum(II) Complexes Containing Aryl Olefins and Quinolines. *J. Coord. Chem.* **2015**, *68*, 3525−3536.
(51) Vicente, J.; Chicote, M. T.; MacBeath, C.; Jones, P. G. Nucleophilic Attack of Carbonyl-Stabilized Phosphorus Ylides on Neutral and Cationic Alkene Platinum(II) Complexes. *Organometallics* **2003**, *22*, 1843−1848.
(52) Huynh, H. V.; Pham, V. T.; Chi, N. T. T. Cyclometallated Platinum(II) Complexes with a Phenylpropene-Derived π/σ-Chelator and N-Heterocyclic Carbenes. *Eur. J. Inorg. Chem.* **2017**, *2017*, 5650−5655.
(53) Cooper, M. K.; Guerney, P. J.; Elder, M.; McPartlin, M. The X-ray Structure of the Complex Dichloroorthovinyldiphenylarsineplatinum(II). *J. Organomet. Chem.* **1977**, *137*, C22−C24.
(54) Cooper, M. K.; Guerney, P. J.; McPartlin, M. The *trans* Influence and *trans* Effect of the Arsine Group. The X-ray Structures of Dichloro[diphenyl(*o*-vinylphenyl)arsine]platinum(II) and [1-(*o*-Diphenylarsinophenyl)-2-methoxyethyl-*As*,C^1]-(hexafluoroacetylacetonato)platinum(II). *J. Chem. Soc., Dalton Trans.* **1980**, 349−354.
(55) Abel, E. W.; Evans, D. G.; Koe, J. R.; Sik, V.; Bates, P. A.; Hursthouse, M. B. Platinum Metal Complexes of Potentially Chelating Alkene-Thioether and Alkene−Selenoethe rLigands: Synthesis and Dynamic Nuclear Magnetic Resonance Study of $[MX_2\{MeE(CH_2)_nCH{=}CH_2\}]$(M = Pt or Pd; X = Cl, Br, or I; E = S or Se; n= 2 or 3) and the X-ray Structure of *cis*-Dibromo(2-thia-6-heptene)platinum(II), $[PtBr_2\{\{MeS(CH_2)_3CH{=}CH_2\}]$. *J. Chem. Soc., Dalton Trans.* **1989**, 985−989.
(56) McCrindle, R.; Ferguson, G.; Arsenault, G. J.; McAlees, A. J.; Ruhl, B. L.; Sneddon, D. W. Reaction of Diazomethane with Platinum(II) Chloride Complexes of Chelating Olefins. Crystal

https://dx.doi.org/10.1021/acs.chemmater.0c03226
Chem. Mater. 2020, 32, 9316−9334

Structure Analyses of *a*-Chloro-*b*-(chloromethyl)-*cd*-(2,2,N,N-tetramethyl-3-buten-1-amine)platinum(II), *a*-Chloro-*b*-(chloromethyl)-*dc*-(2,2,N,N-tetramethyl-3-buten-1-amine)platinum(II), *a*-Chloro-*b*-(chloromethyl)-*dc*-(2,2-dimethyl-3-buten-1-yl methyl sulfide)-platinum(II), and Dichloro[(2,2-dimethyl-4-penten-1-yl)-methylsulfonium methylide-*C*,*C*,*C*]plantinum(II). *Organometallics* **1986**, *5*, 1171−1178.

(57) Abel, E. W.; Evans, D. G.; Koe, J. R.; Sik, V.; Hursthouse, M. B.; Bates, P. A. Platinum Metal Complexes of Potentially Chelating Alkene Thioether and Selenoether Ligands: the Synthesis and Dynamic Nuclear Magnetic Resonance Study of $[MX_2\{E-[(CH_2)_nCR{=}CR_2]_2\}]$(M = Pt or Pd; X = Cl, Br, or I; E = S or Se; n= 2 or 3; R = H or Me) and the X-ray crystal structure of *cis*-Di-iodo-(5-thianona-1,8-diene)platinum(II), $[PtI_2\{S[(CH_2)_2CH{=}CH_2]_2\}]$. *J. Chem. Soc., Dalton Trans.* **1989**, 2315−2321.

(58) Abel, E. W.; Evans, D. G.; Koe, J. R.; Hursthouse, M. B.; Mazid, M.; Mahon, M. F.; Molloy, K. C. Platinum Metal Complexes of Potentially Chelating Alkene−Sulphur and Alkene−Selenium Ligands. The Synthesis by Chalcogen Dealkylation and X-ray Structures of the Dimeric Complexes $[\{PtI(SCH_2CH_2CMe{=}CH_2)\}_2]$ and $[\{PtI(PPh_3)(SCH_2CH_2CM{=}CH_2)\}_2]$, and a DynamicNuclear Magnetic Resonance Study of $[\{PtI(L)(SCH_2CH_2CMe{=}CH_2)\}_2][L = PPh_3, PPh_2Me, or As(CH_2SiMe_3)_3]$. *J. Chem. Soc., Dalton Trans.* **1990**, 1697−1704.

(59) Abel, E. W.; Evans, D. G.; Koe, J. R.; Hursthouse, M. B.; Mazid, M. Dimethylplatinum Complexes of Polydentate Alkene−Sulfur and −Selenium Ligands. *J. Chem. Soc., Dalton Trans.* **1992**, 663−667.

(60) Ermer, S. P.; Struck, G. E.; Bitler, S. P.; Richards, R.; Bau, R.; Flood, T. C. Kinetics and Conformation in the Reversible Insertion of an Alkene into a Platinum-Carbon Bond in a Chelated (Pentenyl) platinum Complex. *Organometallics* **1993**, *12*, 2634−2643.

(61) Zhao, P.; Incarvito, C. D.; Hartwig, J. F. Carbon-Oxygen Bond Formation between a Terminal Alkoxo Ligand and a Coordinated Olefin. Evidence for Olefin Insertion into a Rhodium Alkoxide. *J. Am. Chem. Soc.* **2006**, *128*, 9642−9643.

(62) Albright, T. A.; Hoffmann, R.; Thibeault, J. C.; Thorn, D. L. Ethylene complexes. Bonding, rotational barriers, and conformational preferences. *J. Am. Chem. Soc.* **1979**, *101*, 3801−3812.

(63) Kurosawa, H.; Miki, K.; Kasai, N.; Ikeda, I. In-Plane Olefin Coordination and Unusually Small Substituent Dependency of Stability in (η^3-Allyl) (pentafluorophenyl) (olefin)platinum(II) Complexes. *Organometallics* **1991**, *10*, 1607−1613.

(64) Ziegler, T.; Rauk, A. A Theoretical Study of the Ethylene-Metal Bond in Complexes between Cu^+, Ag^+, Au^+, Pt^0 or Pt^{2+} and Ethylene, Based on the Hartree-Fock-Slater Transition-State Method. *Inorg. Chem.* **1979**, *18*, 1558−1565.

(65) Wright, L. L.; Wing, R. M.; Rettig, M. F.; Wiger, G. R. Molecular Structure of Dichloro(5-methylenecycloheptene)platinum-(II). "In-Plane" Coordination of the Exocyclic Olefin. *J. Am. Chem. Soc.* **1980**, *102*, 5949−5950.

(66) Rakowsky, M. H.; Woolcock, J. C.; Wright, L. L.; Green, D. B.; Rettig, M. F.; Wing, R. M. In-plane Coordinated Double Bonds. Molecular Structures, Spectroscopy, and Stability of 5-Methylenecyclooctene and 5-Methylenecycloheptene Complexes of Platinum(II). *Organometallics* **1987**, *6*, 1211−1218.

(67) Love, R. A.; Koetzle, T. F.; Williams, G. J. B.; Andrews, L. C.; Bau, R. Neutron Diffraction Study of the Structure of Zeise's salt, $KPtCl_3(C_2H_4)^{\bullet}H_2O$. *Inorg. Chem.* **1975**, *14*, 2653−2657.

(68) The second species seen in solution is unlikely to be the isomer in which the two alkyl groups are mutually trans. Trans effects should make such isomers much too high in energy relative to the cis isomers; in addition, without the steric hindrance between the cis double bonds, there would be no reason for the ratio between the two isomers to vary non-monotonically with the length of the carbon backbone, as is seen experimentally. We can also rule out the possibility that the second species is a dimer or higher oligomer: the unusual Pt-C coupling constants seen (especially in **2**) are consistent only with the presence of a bidentate ligand with a small ring size.

(69) Kelly, R. D.; Brent Young, G. Synthesis and Spectroscopic Characteristics of Bis(ethenyldimethylsilylmethyl)platinium(II) Complexes Containing Nitrogen Donor Ligands. *J. Organomet. Chem.* **1989**, *361*, 123−138.

(70) Kelly, R. D.; Young, G. B. Synthesis and Spectroscopic Characteristics of Bis(ethenyldimethylsilylmethyl)platinum(II) Complexes Containing Tertiary Phosphine Ligands. *Polyhedron* **1989**, *8*, 433−445.

(71) Eisenstein, O.; Hoffmann, R. Activation of a Coordinated Olefin toward Nucleophilic Attack. *J. Am. Chem. Soc.* **1980**, *102*, 6148−6149.

(72) Eisenstein, O.; Hoffmann, R. Transition-Metal Complexed Olefins: How Their Reactivity toward a Nucleophile Relates to Their Electronic Structure. *J. Am. Chem. Soc.* **1981**, *103*, 4308−4320.

(73) Still, B. M.; Kumar, P. G. A.; Aldrich-Wright, J. R.; Price, W. S. ^{195}Pt NMR—Theory and Application. *Chem. Soc. Rev.* **2007**, *36*, 665−686.

(74) Clark, H. C.; Manzer, L. E.; Ward, J. E. H. ^{13}C Nuclear Magnetic Resonance Studies of Organometallic Compounds. IV. *cis*-Dimethylplatinum(II) Derivatives. *Can. J. Chem.* **1974**, *52*, 1165−1170.

(75) Brendel, M.; Engelke, R.; Desai, V. G.; Rominger, F.; Hofmann, P. Synthesis and Reactivity of Platinum(II) cis-Dialkyl, cis-Alkyl Chloro, and cis-Alkyl Hydrido Bis-N-heterocyclic Carbene Chelate Complexes. *Organometallics* **2015**, *34*, 2870−2878.

(76) Maudez, W.; Roy, C.; Tran, P. D.; Thurier, C.; Karmous, F.; Doppelt, P. New Dimethyl(norbornadienyl)platinum(II) Precursors for Platinum MOCVD. *Chem. Vap. Depos.* **2014**, *20*, 59−68.

(77) $^1J_{Pt\text{-}C}$ for the olefinic carbons in $(COD)PtR_2$ complexes fall in the order neopentyl (38 Hz) <methyl (40 Hz) <trimethylsilylmethyl (42 Hz) <ethyl (47 Hz) <trifluoromethyl (56 Hz) <benzyl (65 Hz). See Kelly, R. D.; Young, G. B.; M, H.; Clark, H. C.; Manzer, L. E.; Stothers, J. B.; Ward, J. E. H. Carbon-13 Nuclear Magnetic Resonance Studies of Organometallic Compounds. VII. 1,5-Cyclooctadieneplatinum(II) Derivatives. *J. Am. Chem. Soc.* **1975**, *97*, 721−727. Kelly, R. D.; Young, G. B. Synthesis and Spectroscopic Characteristics of Bis(ethenyldimethylsilylmethyl)platinum(II) Complexes Containing Tertiary Phosphine Ligands. *Polyhedron* **1989**, *8*, 433−445. Chisholm, M. H.; Clark, H. C.; Manzer, L. E.; Stothers, J. B.; Ward, J. E. H. Carbon-13 Nuclear Magnetic Resonance Studies of Organometallic Compounds. VII. 1,5-Cyclooctadieneplatinum(II) Derivatives. *J. Am. Chem. Soc.* **1975**, *97*, 721−727.

(78) Hall, J. R.; Appleton, T. G. Complexes with Six-Membered Chelate Rings. III. Factors Influencing the Values of the Platinum-Proton Coupling Constants $^3J_{Pt\text{-}N\text{-}C\text{-}H}$ and $^4J_{Pt\text{-}N\text{-}C\text{-}CH3}$ in Diamine Complexes of Platinum(II) and -(IV). *Inorg. Chem.* **1971**, *10*, 1717−1725.

(79) Karplus, M. Contact Electron-Spin Coupling of Nuclear Magnetic Moments. *J. Chem. Phys.* **1959**, *30*, 11−15.

(80) Gay, I. D.; Young, G. B. Chemical Shift Anisotropy of Organometallic Carbon. *Organometallics* **1996**, *15*, 2264−2269.

(81) Carpentier, J.-F.; Wu, Z.; Lee, C. W.; Strömberg, S.; Christopher, J. N.; Jordan, R. F. d^0 Metal Olefin Complexes. Synthesis, Structures, and Dynamic Properties of $(C_5R_5)_2Zr(OCMe_2CH_2CH_2CH{=}CH_2)^+$ Complexes: Models for the Elusive $(C_5R_5)_2Zr(R)(Olefin)^+$ Intermediates in Metallocene-Based Olefin Polymerization Catalysis. *J. Am. Chem. Soc.* **2000**, *122*, 7750−7767.

(82) Carpentier, J.-F.; Maryin, V. P.; Luci, J.; Jordan, R. F. Solution Structures and Dynamic Properties of Chelated d^0 Metal Olefin Complexes $\{\eta^5{:}\ \eta^1\text{-}C_5R_4SiMe_2NtBu\}Ti(OCMe_2CH_2CH_2CH{=}CH_2)^+$ (R = H, Me): Models for the $\{\eta^5{:}\ \eta^1\text{-}C_5R_4SiMe_2NtBu\}Ti(R')(olefin)^+$ Intermediates in "Constrained Geometry" Catalysts. *J. Am. Chem. Soc.* **2001**, *123*, 898−909.

(83) Stoebenau, E. J.; Jordan, R. F. Nonchelated Alkene and Alkyne Complexes of d^0 Zirconocene Pentafluorophenyl Cations. *J. Am. Chem. Soc.* **2006**, *128*, 8638−8650.

(84) Abel, E. W.; Koe, J. R.; Hursthouse, M. B.; Malik, K. M. A.; Mazid, M. A. Platinum and Rhodium Complexes of Dialkenyl Telluroether Ligands: Synthesis, Dynamic Nuclear Magnetic Reso-

https://dx.doi.org/10.1021/acs.chemmater.0c03226
Chem. Mater. 2020, 32, 9316−9334

nance and Crystal Structure of *cis*-Dibromo(3,3,7,7-tetramethyl-5-tellura-3,7-disilanona-1,8-diene)platinum(II). *J. Chem. Soc., Dalton Trans.* **1994**, 2645−2650.
(85) Reich, H. J. WinDNMR: Dynamic NMR Spectra for Windows. *J. Chem. Educ.* **1995**, *72*, 1086.
(86) Casey, C. P.; Carpenetti, D. W. Measurement of Barriers for Alkene Dissociation and for Inversion at Zirconium in a d^0 Zirconium-Alkyl-Alkene Complex. *Organometallics* **2000**, *19*, 3970−3977.
(87) Casey, C. P.; Carpenetti, D. W.; Sakurai, H. Models for Intermediates in Metallocene-Catalyzed Alkene Polymerization: Alkene Dissociation from $Cp_2Zr[\eta^1,\eta^2\text{-}CH_2Si(CH_3)_2CH_2CH{=}CH_2][B(C_6F_5)_4]$. *Organometallics* **2001**, *20*, 4262−4265.
(88) Frey, U.; Helm, L.; Merbach, A. E.; Romeo, R. High-Pressure NMR Kinetics. Part 41. Dissociative Substitution in Four-Coordinate Planar Platinum(II) Complexes as Evidenced by Variable-Pressure High-Resolution Proton NMR Magnetization Transfer Experiments. *J. Am. Chem. Soc.* **1989**, *111*, 8161−8165.
(89) Wick, D. D.; Goldberg, K. I. C-H Activation at Pt(II) To Form Stable Pt(IV) Alkyl Hydrides. *J. Am. Chem. Soc.* **1997**, *119*, 10235−10236.
(90) Ortuño, M. A.; Conejero, S.; Lledós, A. True and Masked Three-Coordinate T-shaped Platinum(II) Intermediates. *Beilstein J. Org. Chem.* **2013**, *9*, 1352−1382.
(91) Labinger, J. A. Platinum-Catalyzed C−H Functionalization. *Chem. Rev.* **2017**, *117*, 8483−8496.
(92) Yoder, J. C.; Bercaw, J. E. Chain Epimerization during Propylene Polymerization with Metallocene Catalysts: Mechanistic Studies Using a Doubly Labeled Propylene. *J. Am. Chem. Soc.* **2002**, *124*, 2548−2555.
(93) Peng, T. S.; Gladysz, J. A. Mechanism of Equilibration of Diastereomeric Chiral Rhenium Alkene Complexes of the Formula $[(\eta^5\text{-}C_5H_5)Re(NO)(PPh_3)(H_2C{=}CHR)]^+BF_4^-$. The Metal Traverses Between Alkene Enantiofaces Without Dissociation! *J. Am. Chem. Soc.* **1992**, *114*, 4174−4181.
(94) Kelly, W. M.; Wang, S.; Collins, S. Polymerization of Cyclopentene Using Metallocene Catalysts: Competitive Cis- and Trans-1,3 Insertion Mechanisms. *Macromolecules* **1997**, *30*, 3151−3158.
(95) Jones, W. D. Isotope Effects in C-H Bond Activation Reactions by Transition Metals. *Acc. Chem. Res.* **2003**, *36*, 140−146.
(96) Churchill, D. G.; Janak, K. E.; Wittenberg, J. S.; Parkin, G. Normal and Inverse Primary Kinetic Deuterium Isotope Effects for C-H Bond Reductive Elimination and Oxidative Addition Reactions of Molybdenocene and Tungstenocene Complexes: Evidence for Benzene σ-Complex Intermediates. *J. Am. Chem. Soc.* **2003**, *125*, 1403−1420.
(97) Jensen, M. P.; Wick, D. D.; Reinartz, S.; White, P. S.; Templeton, J. L.; Goldberg, K. I. Reductive Elimination/Oxidative Addition of Carbon-Hydrogen Bonds at Pt(IV)/Pt(II) Centers: Mechanistic Studies of the Solution Thermolyses of $TpMe_2Pt(CH_3)_2H$. *J. Am. Chem. Soc.* **2003**, *125*, 8614−8624.
(98) Lersch, M.; Tilset, M. Mechanistic Aspects of C-H Activation by Pt Complexes. *Chem. Rev.* **2005**, *105*, 2471−2526.
(99) Jayaraman, S.; Klein, E. J.; Yang, Y.; Kim, D. Y.; Girolami, G. S.; Abelson, J. R. Chromium Diboride Thin Films by Low Temperature Chemical Vapor Deposition. *J. Vac. Sci. Technol., A* **2005**, *23*, 631−633.
(100) Jayaraman, S.; Yang, Y.; Kim, D. Y.; Girolami, G. S.; Abelson, J. R. Hafnium Diboride Thin Films by Chemical Vapor Deposition from a Single Source Precursor. *J. Vac. Sci. Technol., A* **2005**, *23*, 1619−1625.
(101) Babar, S.; Mohimi, E.; Trinh, B.; Girolami, G. S.; Abelson, J. R. Surface-Selective Chemical Vapor Deposition of Copper Films through the Use of a Molecular Inhibitor. *ECS J. Solid State Sci. Technol.* **2015**, *4*, N60−N63.
(102) Zinn, A. A. Chemical Vapor Deposition of Tungsten. In *The Chemistry of Metal CVD*; Kodas, T. T.; Hampden-Smith, M. J., Ed.; VCH Verlagsgesekhaft mbH and VCH Publishers Inc: Weinheim and New York, 1994; p 147.
(103) Sambles, J. R. The Resistivity of Thin Metal Films—Some Critical Remarks. *Thin Solid Films* **1983**, *106*, 321−331.
(104) Basic Concepts. In *The Electrical Resistivity of Metals and Alloys*; Rossiter, P. L., Ed.; Cambridge University Press: Cambridge, 1987; pp 1−29.
(105) Mayadas, A. F.; Shatzkes, M. Electrical-Resistivity Model for Polycrystalline Films: the Case of Arbitrary Reflection at External Surfaces. *Phys. Rev. B* **1970**, *1*, 1382−1389.
(106) Aaltonen, T.; Rahtu, A.; Ritala, M.; Leskelä, M. Reaction Mechanism Studies on Atomic Layer Deposition of Ruthenium and Platinum. *Electrochem. Solid-State Lett* **2003**, *6*, C130−C133.
(107) Jeffries, P. M.; Dubois, L. H.; Girolami, G. S. Metal-Organic Chemical Vapor Deposition of Copper and Copper(I) Oxide from Copper(I) *tert*-Butoxide. *Chem. Mater.* **1992**, *4*, 1169−1175.
(108) We are not able to trap byproducts quantitatively in our dynamic CVD system, and we are aware that product distributions obtained under static CVD conditions are not necessarily the same as those under dynamic CVD conditions. For **3**, however, the similarity of the structure and properties of the films grown under the two conditions suggests that the product distributions are not likely to be significantly different.
(109) Janssens, T. V. W.; Zaera, F. Neopentyl Iodide on Pt(111) I. Adsorption and Thermal Decomposition. *Surf. Sci.* **2002**, *501*, 1−15.
(110) Lee, T. R.; Whitesides, G. M. Heterogeneous, Platinum-Catalyzed Hydrogenations of (Diolefin)dialkylplatinum(II) Complexes. *Acc. Chem. Res.* **1992**, *25*, 266−272.
(111) Miller, T. M.; Izumi, A. N.; Shih, Y. S.; Whitesides, G. M. Heterogeneous, Platinum-Catalyzed Hydrogenation of (Diolefin)-dialkylplatinum(II) Complexes: Kinetics. *J. Am. Chem. Soc.* **1988**, *110*, 3146−3156.
(112) Miller, T. M.; McCarthy, T. J.; Whitesides, G. M. Deuterium-Labeling Experiments Relevant to the Mechanism of Platinum-Catalyzed Hydrogenation of (Diolefin)dialkylplatinum(II) Complexes: Evidence for Isotopic Exchange via Platinum Surface Hydrogen. The Stereochemistry of Reduction. *J. Am. Chem. Soc.* **1988**, *110*, 3156−3163.
(113) Miller, T. M.; Whitesides, G. M. Isotopic Exchange Reactions Occurring in the Hydrogenation of (1,5-Cyclooctadiene)-dialkylplatinum(II) Complexes Over Platinum Black. *J. Am. Chem. Soc.* **1988**, *110*, 3164−3170.
(114) Cahill, J. J.; Panayotov, V. G.; Cowen, K. A.; Harris, E.; Koplitz, L. V.; Birdwhistell, K.; Koplitz, B. Development of a Method for Investigating Carbon Removal Processes during Photoassisted Film Growth Using Organometallic Precursors: Application to Platinum. *J. Vac. Sci. Technol., A* **2007**, *25*, 104−109.
(115) Geyer, S. M.; Methaapanon, R.; Shong, B.; Pianetta, P. A.; Bent, S. F. In Vacuo Photoemission Studies of Platinum Atomic Layer Deposition Using Synchrotron Radiation. *J. Phys. Chem. Lett* **2013**, *4*, 176−179.
(116) Somorjai, G. A.; Blakely, D. W. Mechanism of Catalysis of Hydrocarbon Reactions by Platinum Surfaces. *Nature* **1975**, *258*, 580−583.
(117) Simonovis, J.; Tillekaratne, A.; Zaera, F. The Role of Carbonaceous Deposits in Hydrogenation Catalysis Revisited. *J. Phys. Chem. C* **2017**, *121*, 2285−2293.
(118) Gozum, J. E. *Transition Metal Allyls and Hydrides as Chemical Vapor Deposition Precursors*; University of Illinois at Urbana-Champaign: Urbana, IL, 1991.
(119) van Lent, R.; Auras, S. V.; Cao, K.; Walsh, A. J.; Gleeson, M. A.; Juurlink, L. B. F. Site-Specific Reactivity of Molecules with Surface Defects—the Case of H_2 Dissociation on Pt. *Science* **2019**, *363*, 155.
(120) Cao, K.; van Lent, R.; Kleyn, A. W.; Kurahashi, M.; Juurlink, L. B. F. Steps on Pt Stereodynamically Filter Sticking of O_2. *Proc. Natl. Acad. Sci. U.S.A.* **2019**, *116*, 13862.
(121) Zhang, P.; Mohimi, E.; Talukdar, T. K.; Abelson, J. R.; Girolami, G. S. Iron CVD from Iron Pentacarbonyl: Growth

https://dx.doi.org/10.1021/acs.chemmater.0c03226
Chem. Mater. 2020, 32, 9316−9334

Inhibition by CO Dissociation and Use of Ammonia to Restore Constant Growth. *J. Vac. Sci. Technol., A* **2016**, *34*, No. 051518.
(122) Babar, S.; Kumar, N.; Zhang, P.; Abelson, J. R.; Dunbar, A. C.; Daly, S. R.; Girolami, G. S. Growth Inhibitor To Homogenize Nucleation and Obtain Smooth HfB_2 Thin Films by Chemical Vapor Deposition. *Chem. Mater.* **2013**, *25*, 662−667.
(123) McDermott, J. X.; White, J. F.; Whitesides, G. M. Thermal Decomposition of Bis(phosphine)platinum(II) Metallocycles. *J. Am. Chem. Soc.* **1976**, *98*, 6521−6528.
(124) Liu, S.; Gray, D.; Zhu, L.; Girolami, G. S. Lithium−Olefin π-Complexes and the Mechanism of Carbolithiation: Synthesis, Solution Behavior, and Crystal Structure of (2,2-Dimethylpent-4-en-1-yl)lithium. *Organometallics* **2019**, *38*, 2199−2210.
(125) *Nuts*; Acorn NMR Inc.: Livermore, CA, 2012.
(126) Reich, H. J. WinDNMR help. https://www.chem.wisc.edu/areas/reich/windnmrhlp/index.htm (accessed June 10th, 2019).
(127) Ammann, C.; Meier, P.; Merbach, A. A Simple Multinuclear NMR Thermometer. *J. Magn. Reson.* **1982**, *46*, 319−321.
(128) Morse, P. M.; Spencer, M. D.; Wilson, S. R.; Girolami, G. S. A Static α-CH$^{\bullet\bullet\bullet}$M Interaction Observable by NMR Spectroscopy: Synthesis of the Chromium(II) Alkyl $[Cr_2(CH_2SiMe_3)_6^{2-}]$ and its Conversion to the Unusual 'Windowpane' Bis(metallacycle) Complex $[Cr(\kappa^2CC'\text{-}CH_2SiMe_2CH_2)_2^{2-}]$. *Organometallics* **1994**, *13*, 1646−1655.
(129) Price, D. M. Vapor Pressure Determination by Thermogravimetry. *Thermochim. Acta* **2001**, *367*−*368*, 253−262.
(130) Sasse, K.; Jose, J.; Merlin, J.-C. A Static Apparatus for Measurement of Low Vapor Pressures. Experimental Results on High Molecular-Weight Hydrocarbons. *Fluid Phase Equilib.* **1988**, *42*, 287−304.
(131) August, E. F. Ueber die Berechnung der Expansivkraft des Wasserdunstes. *Ann. Phys.* **1828**, *89*, 122−137.
(132) Mohimi, E.; Zhang, Z. V.; Mallek, J. L.; Liu, S.; Trinh, B. B.; Shetty, P. P.; Girolami, G. S.; Abelson, J. R. Low Temperature Chemical Vapor Deposition of Superconducting Vanadium Nitride Thin Films. *J. Vac. Sci. Technol., A* **2019**, *37*, No. 031509.
(133) Liu, S.; Zhang, Z.; Abelson, J. R.; Girolami, G. S. "Platinum ω-Alkenyl Compounds as Chemical Vapor Deposition Precursors. Mechanistic studies of the Thermolysis of $Pt[CH_2CMe_2CH_2CH{=}CH_2]_2$ in Solution and the Origin of Rapid Nucleation," Submitted to Organometallics, in press . DOI: 10.1021/acs.organomet.0c00542.
(134) Cheon, J.; Dubois, L. H.; Girolami, G. S. Mechanistic Studies of the Thermolysis of Tetraneopentyltitanium(IV). 2. Solid State and Ultra-High-Vacuum Studies of the Chemical Vapor Deposition of TiC Films. *J. Am. Chem. Soc.* **1997**, *119*, 6814−6820.

NOTE ADDED AFTER ASAP PUBLICATION

This paper was published on the Web on October 27, 2020, with reference 77 missing parts. The corrected version was reposted on October 28, 2020.

https://dx.doi.org/10.1021/acs.chemmater.0c03226
Chem. Mater. 2020, 32, 9316−9334